AMMRC CR 64-07/F

AMMRC CR 64-07/F

SOLIDIFICATION OF IRON BASE ALLOYS AT LARGE DEGREES OF UNDERCOOLING

for October 1, 1966- -December 31, 1967

by

M.C. Flemings M. Myers and W. E. Brower, Jr.

July 15, 1968

Department of Metallurgy and Materials Science
Massachusetts Institute of Technology
Cambridge, Mass. 02139

Contract No. DA-19-020-AMC-0231(X)

ARMY MATERIALS AND MECHANICS RESEARCH CENTER
WATERTOWN, MASSACHUSETTS 02172

The findings in this report are not to be construed as an official Department of the Army position, unless so designated by other authorized documents.

Mention of any trade names or manufacturers in this report shall not be construed as advertising nor as an official indorsement or approval of such products or companies by the United States Government

DISPOSITION INSTRUCTIONS

Destroy this report when it is no longer needed.
Do not return it to the originator.

SOLIDIFICATION OF IRON BASE ALLOYS

AT LARGE DEGREES OF UNDERCOOLING

AMMRC CR 64-07/F

by

M. C. Flemings, M. Myers, and W. E. Brower, Jr.

for

Contract Period
October 1, 1966 - December 31, 1967
Department of Metallurgy
Massachusetts Institute of Technology
Cambridge, Massachusetts 02139

July 15, 1968
DA-19-020-AMC-0231(X)

D/A Project No. 1C024401A328
AMCMS Code No. 5025.11.294
Metals Research for Army Materiel

U. S. Army Materials and Mechanics Center
Watertown, Massachusetts 02172

Abstract

Results are presented of isothermal holding experiments on Fe-50% Cu alloy with silica inclusions present. In addition to rapid dendrite coarsening, the inclusions are "pushed" by the growing dendrites; they collide, join and coalesce, and they coarsen by diffusion (Ostwald ripening). It is probable that similar effects occur during solidification of usual castings and ingots.

A levitation melting, undercooling, and splat cooling device has been modified to permit greater flexibility of operation and to incorporate ability to make chill plate castings (for study of mechanical properties as well as for structure). Dendrite arm spacing of commercial steel alloy castings made in this apparatus varies from about 50 microns for gas cooled specimens to less than 1 micron for splat cooled specimens. In work on Fe-Si-O alloy, no optically visible inclusions have been found in splat cooled samples.

Table of Contents

List of Figures

List of Tables

Chapter 1: INTRODUCTION

Background Research

Research on undercooled iron base alloys has been in progress in this laboratory since 1963. Results have been published in four technical reports and three papers[1-6]. Major aims of the program have been to (1) study effects of undercooling on structure, segregation, and properties of ferrous alloys, and (2) demonstrate that techniques for achieving large degrees of undercooling could be scaled up to relatively large amounts of material and to shaped castings.

A wide variety of ferrous alloys have been undercooled in the course of the research by up to 540°F (300°C) below their melting point. Castings weighing as much as 4 pounds have been undercooled in these large amounts without difficulty. Alloys undercooled have included AISI 4340, AISI 52100, 440C, and Fe-25% nickel. Structure and segregation are significantly affected by the undercooling. The structural refinement resulting from undercooling results in appreciable improvement of ductility of AISI 4330 steel (from 8% to 25% at 200,000 psi yield strength).

A most important fundamental finding was that structure coarsening ("ripening") determines final dendrite arm spacing in melts nucleated at small undercoolings and grain size in melts nucleated at large undercoolings. This finding led to studies

in which it was shown the same factors govern final dendrite arm spacing in usual castings and ingots.

Recent and Current Research

Recent and current research has been concentrated on extending the foregoing to multi-phase alloys, including alloys with inclusion forming elements present.

One portion of the program has been entirely on bulk samples (order of 100 gms). In this portion, extensive work has been completed on structure of undercooled binary eutectics. Current work, reported in detail herein, is primarily on "coalescence", "coarsening" and "pushing" of inclusions during solidification. Work, for experimental convenience is on Fe-Cu alloys with SiO_2 present. Experimental evidence is clear that the three foregoing phenomena ("coalescence", "coarsening", and "pushing" of inclusions) take place during isothermal holding in the liquid-solid zone. The evidence suggests that they also take place during solidification of undercooled and non-undercooled samples. This work is the first that indicates, and measures quantitatively, the importance of the foregoing three phenomena in solidification. A related portion of the program has been on casting undercooled shaped specimens.

A second portion of the program has been on levitation melted, bulk undercooled and/or rapidly solidified specimens. Specimens are "splatted" to achieve cooling rates on the order

of 10^6°C/sec or cast in thin section plate molds to achieve cooling rates the order of 10^4°C/sec. Much of the past year's work has been on apparatus improvement and that work is reported in detail herein. Experiments are currently underway on structural changes obtained at these large cooling rates. Results have shown, for example, that eutectic phases can be completely suppressed and it appears that in many cases inclusion formation can also be suppressed.

An important part of current and planned work in this second phase of the work is measurement of mechanical properties of alloys produced. It appears, for example, that at sufficiently high cooling rate, AISI 4330 alloy can be obtained that is essentially free of microsegregation and inclusions. Mechanical properties of such material are expected to be of considerable technological interest.

References

1. Castings and Solidification Section, Department of Metallurgy, M.I.T., "Solidification of Iron Base Alloys at Large Degrees of Undercooling", U.S. Army Materials Research Agency, Contract No. DA-19-020-AMC-0231(X), Interim Report, October 1, 1963 - September 30, 1964.

2. T. Z. Kattamis, M. C. Flemings, "Solidification of Iron Base Alloys at Large Degrees of Undercooling", U.S. Army Materials Research Agency, Contract No. DA-19-020-AMC-0231(X), Interim Report, October 1, 1964 - September 30, 1965.

3. T. Z. Kattamis, M. C. Flemings, "Solidification of Iron Base Alloys at Large Degrees of Undercooling", U.S. Army Materials Research Agency, Contract No. DA-19-020-AMC-0231(X), Interim Report, October 1, 1965 - September 30, 1966.

4. T. Z. Kattamis, M. C. Flemings, "Dendrite Structure and Grain Size of Undercooled Melts", Trans. Met. Soc. AIME, November, 1966, pp. 1523-1532.

5. T. Z. Kattamis, M. C. Flemings, "Solidification of Highly Undercooled Castings", Trans. AFS, Vol. 75, 1967, pp. 191-198.

6. T. Z. Kattamis, M. C. Flemings, "Structure of Undercooled Eutectics" (to be published).

Chapter 2: MORPHOLOGY, GROWTH, AND MOTION OF INCLUSIONS IN DENDRITIC GROWTH

General

Extensive experimental and theoretical work has been done on mechanisms of formation of inclusions in steel; useful reviews include those referenced[1-5]. Work reported herein deals primarily with silica (SiO_2) inclusions; pertinent works dealing particularly with this type inclusion are those of Benedicts and Lofquist[5], Hilty and Crafts[6], Forward and Elliott[7], and Lindborg and Torsell.[8]

Among the earlier studies of particular relevance are those of Benedicts and Lofquist[5] who distinguished between "exogenous inclusions" (those trapped mechanically in the melt) and "endogenous inclusions" (those precipitated from the melt). We will use these terms and distinguish further between two types of endogenous inclusions; (1) "primary inclusions" or "primary deoxidation products" (those that form from the melt prior to solidification of the iron dendrites), (2) "secondary inclusions" or "secondary deoxidation products" (those that form during solidification of the iron dendrites).

Much early cataloguing of inclusions was done by Herty and co-workers, with their many papers on the subject compiled in a memorial volume in 1957[9]. Herty recognized at an early date that inclusion chemistry and morphology were intimately related to solidification mechanism and constructed from experiment many relevant binary oxide phase diagrams.

Hilty and Crafts extended this type of analysis to the ternary system Fe-O-S and classified resulting inclusions as Type I, II, and III, depending on the initial S/O ratio and hence on the compositional path followed by the liquid (solute redistribution) during solidification[10,11]. Other workers have performed similar basic studies relating inclusion morphology to the multicomponent phase diagram in the Fe-O-S system[12] and in other systems including Fe-Mn-S[13], Fe-Mn-O-S[14], and the simple ternary system of most relevance to this work, Fe-Si-O[7].

In addition to the more fundamentally oriented studies on inclusions noted above there has been a very large number of applied studies relating inclusion morphology to metal gas content and/or details of deoxidation practice. Some of these have been outgrowths of the fundamental studies above and others have been purely empirical in nature. Several of the more general papers on the subject are referenced[16-18].

The engineering interest in inclusions stems from the major effect these are known to have on fracture behavior of cast and wrought steel. It is clear that not only the amount of inclusions is important, but also their morphology, the deformation behavior of the inclusions, and the strength of the interface between the inclusions and the matrix[19-21].

Major improvements have been made in the properties of cast and wrought steel through control of amount and type of

inclusions. The improvements have come about largely as a result of empirical studies such as those cited above, often with application of such understanding of solidification mechanisms as was available at the time (e.g., work of Sims and Briggs[16]). It seems clear that additional major improvements in inclusion control are feasible through application of modern solidification ideas to inclusion studies, and it is to this end that the current study is devoted (with emphasis on one particular and important type of inclusion, SiO_2. The remainder of this Introduction is concerned with some aspects of previous inclusion studies that are particularly relevant to the current work.

Formation of Primary Endogenous Inclusions

During cooling of steel from above its melting point, saturation of inclusion forming elements may be reached before solidification of the iron. For example, if equilibrium is reached according to the reaction

$$\underline{Si} + \underline{2O} \rightleftarrows SiO_2$$

at, say 1600°C, then on subsequent cooling to the solidification temperature, the melt must be either supersaturated with respect to SiO_2 or must precipitate SiO_2 on the crucible wall or in the bulk as inclusions. Researchers have proposed that large supersaturations are required to precipitate the inclusions, but the evidence is very strong that these "primary endogenous

inclusions" generally require very little supersaturation for their formation.

As one example, iron melts equilibrated with SiO_2 at about 50°C above their melting point always contain large SiO_2 inclusions which seem certain (as discussed above) to have come from the melt during cooling, but before formation of the iron. Simple calculations show that in order for the inclusion to have formed in the melt, the supersaturation required must have been small - certainly far less than that required for "homogeneous nucleation"[22]. Related experiments on other systems, including those of Turpin and Elliott[23], Brower[12] and Yarwood[13], show directly for the Fe-Cu-Si-O and Fe-O-S systems that no significant undercooling occurs before nucleation of the primary inclusions.

Thus, it seems that primary endogenous inclusions form by heterogenous nucleation* from the liquid at very little supersaturation or by growth of random enbryos which become critical nuclei as the melt cools. Following this formation, growth and coalescence is rapid. As example, Torssell[25] has studied the growth and separation of silica particles in liquid iron. Samples were taken from a 0.6 kg iron bath at various times after the addition of silicon. By a particle-counting technique developed by Bergh and Lindberg[26] the size distribution

---

* or, in some cases, perhaps by spinodal decomposition[24].

of the inclusions was determined. The number of particles at the first sampling, 10 sec. after silicon addition, was of the order of 3×10^7 to 10^8 per cu cm, the largest particles having a radius of 2 to 4 microns. The volume fraction was 0.001 to 0.004; i.e., the dispersion was very dilute. During subsequent holding the largest particles increased their radius by a factor of 10 after about a minute, and the whole size distribution was displaced toward larger values.

Particle coarsening or coalescence such as that described above has been recognized by many workers, and mechanisms proposed for the coarsening have included:

1. diffusion coarsening (Ostwald ripening)[8],
2. coalescence following collisions which result from:
   a. differential settling rate of inclusions of different size or density ("Stokes collision")
   b. local velocity gradients in the liquid bath ("gradient collisions")[8]
   c. Brownian motion ("Brownian collisions")[27]
   d. electrostatic attraction[9].

Following the recent work of Lindborg and Torsell[8] it seems most likely that "Stokes collisions" account for the major part of particle coarsening in primary inclusions, although at long holding times it is evident that diffusion coarsening must become important.

An aspect of inclusion coarsening not heretofore considered is how two inclusions "coalesce" (sinter) into a single inclusion once they have collided. For the liquid or glassy SiO_2 inclusions of interest herein we propose a viscous flow model after Frenkel[28,29]. One or another of the various diffusional models for sintering may well be more appropriate in other types of inclusions.

Formation of Secondary Endogenous Inclusions

By no means do all inclusions form prior to solidification of the iron phase and, if the melt is sufficiently pure, no primary inclusions form. During solidification, however, interdendritic liquid becomes enriched in alloy elements and impurities. At some point during solidification inclusions ("secondary endogenous inclusions") then form*, even in very pure, vacuum melted material. These secondary inclusions are generally thought to be distinquishable from primary inclusions by the following characteristics[9,30,31]:

1. They are usually much smaller than inclusions taken to be primary (e.g., one often finds in a given ingot two different populations of inclusions, one greater than about 10 microns, and one less than about three microns; the smaller population is assumed to be secondary)[9,30].

---

* A sound quantitative treatment of how microsegregation of alloy elements leads to inclusion formation in steel has been given by Turkdogan[33].

2. The size of the smaller population above (secondary) is a strong function of solidification rate, whereas the size of the larger (primary) is not[31].

3. The smaller inclusions are often primarily at dendrite arm boundaries whereas the larger are not.

4. Certain of the smaller inclusions have shapes characteristic of solidification of remnant interdendritic liquid (e.g., Type II sulphides).

There has been some recent discussion in the literature on the question of whether secondary inclusions nucleate with little supersaturation or whether, in fact, sufficient supersaturation is required to achieve "homogeneous nucleation". The point has been made that even though primary inclusions may nucleate with little undercooling on existing impurity particles, after dendritic solidification begins the melt is subdivided into many individual interdendritic "droplets" and it is unlikely that each little isolated pool, would possess its own effective nucleation site[7,21]. On the other hand, it is clear that individual pools are not diffusionally isolated from their immediate neighbors until quite near the end of solidification. Further, if there are anything like the 10^7 to 10^8 nucleating sites per cm^2 as suggested by Torssell and Lindborg[8], there are ample nuclei to provide a nucleus per dendrite at usual solidification rates. Experiments have not as yet resolved the question of extent of supersaturation required for formation of secondary incluions.

As noted above, it has been clear for some time that the size of secondary inclusions is a function of cooling rate; limited quantitative studies have been made, of this effect, but no work has been done (prior to that reported herein) to interpret the cause of the coarsening occuring at slow cooling rates.

Also as noted above, secondary inclusions often occur at or near dendrite arm boundaries, rather than randomly throughout the matrix. This may (and in many cases certainly is), a result simply of the fact that they formed late in solidification. It is possible however, that inclusions which form at an early or intermediate stages of solidification are "pushed" by the advancing front of a thickening dendrite arm so that they end up at interdendritic spaces even though they first formed at some other location. Experiments illustrating such "pushing" have been performed using transparent organic melts by Uhlmann, Chalmers and Jackson, and a mechanism proposed[32].

The experiments showed that for a given matrix material, particle size, and particle type, there was a given critical interface velocity, v_c, below which the particles were pushed ahead of the interface and not trapped by it. For particles below about 15 microns diameter, the critical velocity was independent of particle size. Essential experimental results of this study are given in Table 1. These results are of particular relevance to studies of inclusions since, as will be shown later, (1) pushing of particles by metallic melts should

take place at and below critical velocities of the same order as observed for the organic melt, and (2) interface velocities in dendritic growth of iron melts are substantially below the critical velocities in Table 1 required for pushing.

Experimental Procedure

In order to perform the types of coarsening experiments reported herein, it was necessary to employ an alloy of a wide freezing range (so small temperature differences would not result in large differences in fraction solid). The base alloy chosen was Fe-50% Cu alloy, which freezes over a range of 336°C, Figure 1. The curve of fraction solid versus temperature for this alloy*, Figure 2, shows that about 50% of the solid forms during the first 50°C of solidification, with the remaining 50% freezing over a range of about 290°C.

The base alloy of iron-50% copper was made of "Ferrovac E" iron (99.98% purity) and pure copper (99.999% purity). A small quantity of silicon (.05%) was added as one of the inclusion forming elements; this was 99.9% pure, with the major impurity being iron. Charge materials were weighed and the iron and copper cleaned by grinding.

---

* Calculated from the "non-equilibrium lever rule" which assumes complete liquid diffusion equilibrium over distances the order of interdendritic spaces, except for the assumption of no solid diffusion[37].

Melting was in a Balzer vacuum melting and pouring unit, in a silica crucible with graphite susceptor; charge weight was 450 grams. Crucible was cleaned with acetone and charged with Fe, Cu, and Si. The furnace was then evacuated to 50 microns, backfilled with He to 1/2 atm. and melting began.

The charge was melted and superheated to 1550°C within 15 minutes, held isothermally at 1550°C for 20 minutes to allow equilibration of the melt with the SiO_2 crucible. Power was then turned off and the melt allowed to cool in-situ. At approximately 1530°C an iron wire was plunged into the melt to prevent any possible undercooling before solidification at the liquidus (approximately 1430°C). Temperatures were measured with a Pt-Pt 10% Rh thermocouple in a silica protection tube immersed in the melt.

To be certain of ingot homogeneity, and equilibration with the SiO_2 crucible, the ingot was then cut into pieces approximately 3/4" x 3/4" x 1-1/2" and the above melting equilibration and cooling procedure repeated. Portions of the ingot that were at the bottom of the first crucible were charged at the top in the second melting.

Coarsening experiments described below were carried out on sections of the master weighing approximately 50 grams. Each individual series of experiments (i.e., isothermal holding at 1275°C) was carried out using material from roughly

the same height in the same master. After cutting a section from the master, a hole was drilled in it for insertion of the thermocouple (in a silica protection tube). The sample was then placed in a silica crucible (1" dia. x 3" high), thermocouple inserted and melting procedure followed as for the master (furnace evacuated to 50 microns, backfilled to 1/2 atm. of He before melting).

The specimens were not, however, completely melted. They were simply heated to the isothermal holding temperature and held there for times of 1/2 hr., 2 hrs., and 4 hrs. Two holding temperatures were used: (1) 1400°C, at which temperature the alloy is approximately 42% solid (Figure 2), and (2) 1275°C, at which temperature the alloy is approximately 50% solid. After isothermal holding, furnace power was cut off the specimen cooled at approximately 1°C/sec through the solidification range.

After removal from the furnace, specimens were examined metallographically; typical microstructures are shown in Figures 3-8. No etching was necessary. The following measurements and observations were made and discussed below.

a. Secondary dendrite arm spacing.
b. Volume fraction of inclusions.
c. Number of inclusions per unit area.
d. Number of inclusion "members" per unit area.
e. Number of inclusion "members" per inclusion.

f. Apparent inclusion size.

g. Apparent inclusion "member" size.

h. Inclusion location, i.e., whether the inclusions were in the primary (iron-rich) dendrites or in the second phase (copper-rich).

The difference between "inclusions" and "inclusion members" is described as follows. Briefly, many inclusions were observed to be made up of contiguous but distinct regions - as if small spherical incluions had collided and were in the process of sintering together. Each distinct approximately sphere-like region within an inclusion is termed herein an "inclusion member".

Secondary dendrite arm spacings were measured using procedures previously described[35]. For each result reported, measurements were made of dendrite spacings in at least 10 different grains on photomicrographs at 55X. Measurements were made and reported for both horizontal and vertical sections.

Measurements of volume per cent inclusions was done by quantitative metallography. A two-dimensional systematic point count was used following procedure of Cahn and Hilliard[36]. A systematic array of points was used, provided by the corners of a two-dimensional lattice. A 7 x 10 grid having 70 points was placed on photomicrographs of the structure to be analyzed; the photomicrographs were at 305X.

A coarse-mesh lattice criteria was satisfied, whose condition is the following:

$$p_0 + p_1 = 1$$

$$p_n = 0 \quad \text{for} \quad n \geq 2$$

where p_n is the probability that a feature will occpy n lattice points. The relationship between standard deviation and the number of points falling on the features, as calculated by Cahn and Hilliard is given by:

$$\sigma_{np}^2 = \bar{N}_p \text{ or } \left(\frac{\sigma_{nf}}{\bar{N}_f} \right)^2 = \frac{1}{\bar{N}_p} \qquad (1)$$

where σ = standard deviation

$\bar{N}_p$ = number of points falling in the feature

$\bar{N}_f$ = $\bar{N}_p/N$

also $\bar{N}_p$ = Nv_f, v_f being volume fraction of the feature

N = total points applied

For each result reported, 124 different (non-overlapping) photomicrographs were made of each specimen. Thus at 305X .1 cm^2 was observed for each specimen. Photomicrographs were taken near the vertical center-line of the sample from top to bottom. The above grid was placed once on each photomicrograph and the fraction of grid points falling on each inclusion noted - this fraction giving directly the volume fraction inclusions. A total of 8680 points were so

counted. Resulting standard deviation for volume fractions reported are less than .05% as calculated by Cahn and Hilliard's expression (equation 1) for a two-dimensional coarse-mesh systematic point count method.

To report the number of inclusions per unit area, the total number of incluions on all 124 different photomicrographs were counted (and divided by the total area covered). The number of inclusion "members" per unit area and number of inclusion "members" per inclusion were similarly counted directly on all 124 different photomicrographs.

"Apparent inclusion size" and "apparent inclusion member size" were also measured directly from all 124 films. The largest dimension of each inclusion was individually measured and recorded as "apparent inclusion size". The approximate diameter of each member of every inclusion was measured and recorded as "apparent inclusion member size".

Finally, the location of each inclusion was noted and recorded (i.e., whether it was in the primary dendrite or secondary surrounding phase).

Results

Results of the structure examinations on the master and isothermally coarsened alloys are summarized in Figures 3-13 and discussed individually below. Figures 3-8 show typical photomicrographs of the various samples, some general

observations being the following:

1. Significant dendrite coarsening occurs during isothermal holding, and coarsening is significantly more rapid at 1400°C than at 1275°C. No significant difference is noticed between spacings in horizontal and vertical sections. (Table 2 summarizes measurements of dendrite arm spacings.)

2. Inclusions are clearly evident in most photomicrographs; the vast majority of these are not in the iron dendrites but rather in the copper-rich second phase. This is true in spite of the great amount of dendrite coarsening taking place. The conclusion seems inescapable that, for some reason, inclusions are not incorporated in the surviving and growing dendrite arms.

3. Many of the inclusions which lie adjacent to the iron dendrites rest in concavities of the dendrites - as if in the coarsening process growth was slower beneath the inclusions than in adjacent regions.

4. There appear to be areas where the density of inclusions is much higher than elsewhere (where groups of a half dozen or more inclusions are near each other but not touching).

5. There are clearly regions where groups of sphere-like inclusions are touching one another to form a larger inclusion (in our terminology these are now inclusion "members" comprising a larger "inclusion").

6. Some large non-spherical inclusions seem to have "members" which are not just touching but are in various stages of sintering together.

7. On the vertical sections many more inclusions are seen to lie just below the iron-rich dendrites than just above. The inclusions give the impression of having "floated up" until they were stopped by the iron dendrites.

8. With increasing holding time, inclusions become much fewer in number and those present become larger in average size. At the longer holding times, the process of sintering (or "coalescence") of groups of inclusion members is much more complete.

Systematic point counting analysis for volume fraction inclusions was done on all specimens and has been completed for the master and the two samples isothermally coarsened at 1400°C. In all these cases, the results yield 0.26 volume percent inclusion (variance .0025%) indicating no gain or loss of silicon during coarsening. Taking density of the silica inclusion as 2.2 gm/cm^3, the density of the iron dendrites as 7.9 gm/cm^3 and that of the copper-rich matrix as 9.0 gm/cm^3, this volume percent is equivalent to approximately .067 wt. %. Results of chemical analyses also indicated weight percent SiO_2 and Si in solution were constant during the coarsening experiments (Table 3). However, the weight percent SiO_2 given by chemical analysis (approximately .03%) is significantly different than that given

by point counting, and causes of this discrepancy are now being studied.

Figure 9 shows the size distribution of single-membered inclusions in the second phase before and after isothermal coarsening at 1400°C. The bar graphs show clearly that coarsening is taking place; the mean apparent diameter increases from 2.83 microns in the master to 3.45 microns in the specimen coarsened 2 hours. The total number of inclusions decreases significantly during coarsening: 1100 in the master; 708 in the sample coarsened 1/2 hour, and 431 in the same coarsened 2 hours. In this figure, only single membered inclusions are considered, in an attempt to separate any possible diffusional coarsening ("Ostwald ripening") effects from other types of coarsening; this is discussed more in a later section.

Inclusions within the iron dendrites are also omitted in this figure, under the assumption that such inclusions would have had little chance to coarsen. These inclusions comprised a small fraction of the total (less than 10% in the master); the mean size in all three specimens studied was about 3 microns. Results on size distribution of these inclusions are given in Table 4.

Figure 10 shows similar data to Figure 9, except for all inclusion "members" (in single, as well as multi-membered, inclusions). This figure, like the previous shows a coarsening of members and a decrease in number. The shape of the distribution curve is, however, somewhat different.

Figure 11 summarizes data from the preceding two figures; it shows mean apparent diameters versus time and illustrates in a different way the coarsening taking place. Figure 12 similarly shows the decrease in number of inclusions, and inclusion members with coarsening time.

Figure 13 gives members per inclusion before and after isothermal coarsening at 1400°C. With coarsening, the number of single membered inclusions decrease and multi-membered inclusions increase - clear evidence of collisions of some sort taking place.

Discussion

One obvious result of the isothermal holding experiments described in the previous section was the increase in spacing of the secondary dendrite arms with increasing holding time. Table 2 shows this increase and shows further that the rate of coarsening at 1400°C (42% solid) is greater than that at 1275°C (50% solid). This behavior is as predicted by Coughlin, Flemings and Kattamis[35] who showed, on the basis of a simple model, that the critical time for significant coarsening to occur, t_c, is given by the following approximate relation:

$$t_c \simeq \frac{HC_L(1 - k)md^3}{\sigma DT} \qquad (2)$$

where H = heat of fusion per unit volume

C_L = composition of liquid in equilibrium with solid

k = C_S/C_L

T = temperature (absolute)

m = slope of liquidus at T

d = secondary dendrite arm spacing

D = diffusion coefficient in liquid

σ = solid-liquid interfacial energy

Solution of (2) using constants given in Table 5 yields times of about 9000 seconds (2-1/2 hours) for coarsening at 1400°C. This time is the order of that in which significant coarsening was observed experimentally. Also in qualitative agreement with experiment is the fact that coarsening is predicted to be slower at the lower temperature, 1275°C. The predicted decrease is large (about a factor of 8) because of the larger change in slope of the liquidus in going to the lower coarsening temperature. The experimental decrease in coarsening rate is somewhat smaller than this, being only about a factor of 3-4 (from the data of Table 2).

Examination of the photomicrographs of Figures 3 through 8, and of the data presented in Table 4 and Figures 9 through 13 shows that there is not only a great difference in the number of trapped and untrapped inclusions but also a distinct difference in behavior between inclusions which are trapped in the iron-rich dendrites and those which are located in the copper-rich second phase. The latter inclusions tend to increase in size and to decrease in number with increasing

holding time at 1400°C, while the former remains constant in number and size. Two inferences may be extracted from these statistical findings. One is that most trapped inclusions become so during the initial solidification of the master ingot (and not released by subsequent coarsening). The other is that many inclusions located after solidification in the copper-rich second phase were rejected by the advancing solid-liquid interface of the coarsening dendrite arms.

A probable mechanism for this rejection has been discussed by Uhlmann et al[32]. They performed experiments on this problem using non-metallic systems. As discussed in the Introduction to this report, the most significant result of their work is that for most of the systems there exists a critical growth velocity below which inclusions will not be trapped. This critical velocity is thought to be a function of such material properties as surface energy, surface smoothness, particle size, viscosity and diffusion coefficient of the liquid. It is of interest that these properties are not greatly different for the metal-silica system studied herein than for most of the materials studied by Uhlmann et al. We therefore infer that there exists for the coarsening dendrites a critical growth velocity of the same order as those in Table 1, above which inclusions will be trapped and below which they will be pushed.

Next, it is of interest to estimate the microscopic growth rate (dendrite arm thickening rate) obtained in this study. From Figures 3 and 8 we see that dendrite arm thickness

increases from 16 microns to 54 microns in two hours holding at 1400°C. Assuming cylindrical arms, this corresponds to a growth rate of about 3×10^{-7} cm/sec, far smaller than any of the critical velocities noted in Table 1. Thus, based on comparison of experimental results alone, it is reasonable that our inclusions, like those of Uhlmann et al should be pushed ahead of the advancing liquid-solid interface.

The following formulation for determining critical growth velocity, derived from theory by Uhlmann et al, has been found to agree[32] within an order of magnitude with experimental results:

$$v_c = \frac{1}{2}(n+1)\left(La_o V_o \frac{D}{kTR^2}\right) \qquad (3)$$

where n = a constant near 5

L = heat of fusion per unit volume

a_o = lattice constant = 3×10^{-8} cm

$V_o = a_o^3$ = atomic volume = 27×10^{-24} cm^3

D = diffusion constant in liquid

k = Boltzmann's constant

T = temperature (absolute)

R = inclusion radius

A solution of equation (3) for the system under consideration in this work is shown in Table 6. According to this solution $v_c = 9.7 \times 10^{-4}$ cm/sec for our system.

Based on the above, we expect essentially all inclusions in the liquid to be pushed ahead of the growing dendrite arms during isothermal coarsening. We further expect most inclusions to be pushed ahead during usual solidification since the velocity of thickening of dendrite arms in solidification of usual castings and ingots is also considerably lower than the "critical velocity" for pushing cited above. However, those inclusions that lie directly in front of, or adjacent to, a rapidly advancing primary arm should be trapped. The small number of inclusions we observed within the iron dendrites in our work were nearly all at or close to the spine of a primary arm.

The location of many inclusions in dendrite concavities may have two explanations. Since the inclusions have a strong tendency to float upward in the liquid (density ratio $\frac{\rho_{liquid}}{\rho_{SiO_2}} \simeq 3.5$), it seems likely that they will come to rest in concave surfaces formed by the dendrites (see Figure 3, vertical section 500X). Alternatively, however, the presence of the particle may have caused the concavity by slowing diffusion of solvent to the growing liquid-solid interface.

Another of the more prominent phenomena observed by these experiments was areas of high inclusion density usually located between dendrite arms on the lower side of these dendrites. It appeared that the dendrite had blocked further floating of these inclusions (Figure 3).

In the master, there were many inclusions of one or two members, whereas after holding there were fewer inclusions but these few contained many members (Figures 3, 4, 5, etc.). Quantitative data on these observations are presented in Figures 9 through 13. We suggest these areas of high inclusion density result in the following ways:

1. Growing dendrites sweep through already existing inclusions (mostly single membered) trapping a few but pushing most along. Thus, areas of high inclusion density are created at the peripheries of growing dendrite arms.

2. Floating inclusions are led by the shape of the interdendritic network to these same interdendritic regions.

3. Inclusions which come into contact with one another during growth of the iron dendrites begin to sinter as discussed below. Since impinging inclusions stick, it seems likely that the more inclusions a region contains, the more likely it is that other floating inclusions will become caught by impinging upon previously caught members.

Figures 3 through 8 show multi-membered inclusions at various stages of the sintering process. The process of sintering together, or coalescence, begins as soon as the inclusions come into mechanical contact. This problem has been treated by in general by Frenkel[29] and applied to silica by Seward, Uhlmann and Turnbull[29]. Frenkel's equation for the minimum time for complete coalescence of two spheres is:

$$t_c = \frac{r\eta}{\sigma} \qquad (4)$$

where: r = particle radius

η = viscosity

σ = interfacial energy

A solution of equation (4) for the system being studied is shown in Table 7. For two silica spheres of 3 microns diameter at 1400°C, t_c equals about 1-1/2 hours. Since t_c represents the time for coalescence with maximum driving force (surface area per unit volume) which obtains only during the very earliest stages of coalescence, and since collisions may occur over a range of time, it is reasonable to expect that complete coalescence would not be observed (except for very small inclusions) after just two hours holding time. Thus, it is concluded that the majority of single-membered inclusions have been single-membered throughout the experiment. This is useful in interpreting the data of Figures 9-13.

Figure 12 shows that with increasing holding time the number of all inclusion members decreases (including single-membered inclusions). Three possible explanations are evident for this decrease in number of inclusion members. First is the possibility that members disappear by floating out or by dissolving in the melt. However, results of chemical analysis and of point counting indicate that the volume fraction does not change with time, thus ruling out this possibility.

Second, it might be thought that many of the inclusions which came into contact early sinter completely into a single inclusion member. This, as discussed above, is unlikely to account for the total decrease in number of members. The final and most probable explanation is classical diffusional coarsening (Ostwald ripening).[8,9,25,35,38,39]

The mechanism of diffusional coarsening requires that large inclusions grow (increase their radii) at the expense of dissolving smaller particles. Driving force is the overall decrease of surface energy per unit volume inclusion. This phenomenon has been recently studied for dendritic growth by Flemings et al[35], and was investigated for inclusions during deoxidation (and prior to solidification) by Torsell et al[8,25]. They found this mechanism of coarsening was not significant prior to solidification because of the short time involved. Application of the classical analysis for diffusional coarsening (as used also by Torsell and Lindborg[8]) to the experiments herein described produces good agreement with our experimental results. The equation used is derived from the work of Greenwood[38] and Lifshitz and Slyozov[39].

$$r^3_{(t)} = r^3_{(0)} + \alpha\left(\frac{2\sigma V_m C_o D}{RT(C_p - C_o)}\right)t \qquad (5)$$

where: t = coarsening time

$r(t)$ = radius at time t

α = a constant

σ = surface energy

V_m = molar volume of diffusing element

C_o = concentration of diffusing element

C_p = concentration of diffusing element in the particle

D = diffusion coefficient in liquid

R = universal gas constant

T = temperature (absolute)

The sample calculations as applied to this work are shown in Table 8 and are plotted together with experimental results in Figure 14. Since the apparent mean diameter is no doubt smaller than the actual mean diameter[26] actual agreement is somewhat better than that indicated in Figure 14.

Conclusions

1. Dendrite coarsening occurs in Fe-50% Cu alloy during isothermal holding; driving force is reduction of surface area per unit volume. Coarsening is considerably more rapid at 1400°C than at 1275°C, due primarily the large difference in liquidus slope at these two temperatures.

2. Silica inclusions are "pushed" ahead of the dendrite arms that grow during coarsening. Few are trapped by the progressing liquid-solid interface. The inclusions also tend to float during coarsening until stopped by iron-rich dendrites.

3. Silica inclusions in the alloy studied are composed of single or multiple readily distinguishable "members". As coarsening progresses, multi-membered inclusions increase in number while single membered inclusions decrease. It is therefore concluded that inclusion members are joining as a result of "collisions". The "collisions" occur as a result of (a) sweeping action of the coarsening dendrites, (b) differential rates of floating of inclusions of different sizes, and (c) "channeling" of floating incluions by the dendritic network.

4. Total number of inclusions and of inclusion members decreases during isothermal holding. Sizes of individual inclusion members and inclusions increases. It is concluded that "diffusional coarsening" (Ostwald ripening) of inclusions is taking place at measurable rate.

5. Inclusions which "collide" to form a multi-membered inclusion, gradually coalesce by sintering, but in the experiments conducted, sintering does not go to completion.

6. Simple calculations are presented for estimating extent of dendrite coarsening, inclusion "pushing", inclusion sintering, and diffusional coarsening. Results are in qualitative agreement with experiment.

7. It is probable that above conclusions on pushing, joining, coalescing, and diffusional coarsening of inclusions apply as well to solidification of usual castings and ingots.

References

1. C. E. Sims, "The Non-Metallic Constituents of Steel", Trans. AIME, Vol. 215, 1959, p. 367.

2. C. E. Sims, "Non-Metallic Inclusions", Chapter 21 of Electrical Furnace Steel Making, Vol. II: Theory and Fundamentals, Trans. AIME (John Wiley), 1963.

3. R. Kiessling and N. Lange, Non-Metallic Inclusions in Steel, Part I, Iron and Steel Institutes, 1964; Part II, 1966.

4. M. Baeyertz, Non-Metallic Inclusions in Steel, A.S.M., Cleveland, Ohio, 1947.

5. C. Benedicts and H. Lofquist, Non-Metallic Inclusions in Iron and Steel, Chapman and Hall, London, 1930.

6. D. C. Hilty and W. Crafts, "Solubility of Oxygen in Liquid Iron Containing Silicon and Manganese", Trans. AIME, Vol. 188, 1950, pp. 425-436.

7. G. Forward and J. F. Elliott, "Nucleation of Oxide Particles During Solidification", J. Metals, Vol. 19, No. 5, May 1967.

8. U. Lindborg and K. Torssell, "A Collision Model for the Growth and Separation of Deoxidation Products", Trans. Met. Soc. AIME, Vol. 242, 1968, pp. 94-102.

9. C. H. Herty, Jr., Deoxidation of Steel, a Memorial Volume, AIME, 1957.

10. D. C. Hilty and W. Crafts, "Liquidus Surface of the Fe-S-O System", Trans. AIME, Vol. 194, 1952, pp. 1307-1312.

11. W. Crafts and D. C. Hilty, "Sulfide and Oxide Formation in Steel", Elec. Furnace Steel Proc., Vol. 11, 1953, pp. 121-145.

12. W. E. Brower, M.I.T., current research.

13. J. Yarwood, M.I.T., current research.

14. R. Vogel and W. Hotop, "Das Zustansschaubild Eisen-Eisensulfid-Mangan", Archiv. für das Eisenhuttenwesen, Vol. 11, 1937, pp. 41-45.

15. H. Wentrup, "Die Bildung von Eisenschlussen in Stahl", Technische Mitteilungen-Krupp, Heft 5, 1937, pp. 131-142.

16. C. E. Sims and C. W. Briggs, "Effect of Various Deoxidizers on Cast Steel", Elec. Furnace Steel Proc. AIME, Vol. 17, 1959, p. 104.

17. W. Dahl, H. Hangstemberg, and C. Duren, "Conditions for the Occurance of the Various Types of Sulfide Inclusions", Stahl and Eisen, Vol. 86, 1966, No. 13.

18. Y. Miyashita, "Kinetics of Chem. Reaction in Silicon Deoxidization of Steel", 97th AIME Annual Meeting, 1968.

19. Scheil, Schnell, "Deformability of Slag Inclusions in Steel and Its Significance in Evaluation of Forging", Stahl and Eisen, Vol. 72, 5 June 1952, pp. 683-687.

20. R. Kiessling and N. Lange, "Intergranular Brittleness of Cast Chromium Steels", Jl. of Iron and Steel Inst., Vol. 201, 1963, pp. 761-762.

21. R. J. Warrick and L. H. Van Vlack, "Plastic Deformation of Non-Metallic Inclusions Within Dilute Metals", ASM Trans. Quart., Vol. 57, No. 3, September 1964.

22. G. E. Forward, "Nucleation of Oxide Inclusions During Solidification of Iron", Sc.D. Thesis, Department of Metallurgy, M.I.T., 1966.

23. M. L. Turpin and J. F. Elliott, "Nucleation of Oxide Inclusions in Steel", Jl. of Iron and Steel Inst., Vol. 204, 1966, p. 217.

24. J. W. Cahn, "Spinodal Decomposition", Trans. AIME, Vol. 242, February 1968, pp. 168-180.

25. K. Torssell, "Removal of Inclusions Resulting from Deoxidation of Iron with Silicon", Jernkontorets Ann., Vol. 151, 1967.

26. S. Bergh and O. Lindberg, "Microscopic Determination of the Number and Distribution of Non-Metallic Inclusions", Jernkontorets Ann., Vol. 146, 1962, pp. 862-868.

27. Y. Miyashita, "On a Model Concerning Growth of Non-Metallic Inclusion Particles", Nippon Kokan Tech. Rept., Vol. 4, 1965, pp. 41-46.

28. J. Frenkel, "Viscous Flow of Crystalline Bodies Under the Action of Surface Tension", J. Phys. USSR, Vol. 9, No. 5, 1945, pp. 385-391.

29. T. P. Seward III, D. R. Uhlmann, and D. Turnbull, "On the Development of Two-Phase Structure in Glasses with Special Reference to the System $BaO-SiO_2$", Technical Report No. 15 to Office of Naval Research, January 1968.

30. A. Hultgren, "The Origin of Silicate Inclusions in Basic Electric-arc-furnace - Steel of Higher Carbon Contents", Metals Technology, Vol. 15, 15 August 1948.

31. C. A. Zapffe and C. E. Sims, "Silicon-Oxygen Equilibrium in Liquid Iron", Trans. AIME, Vol. 154, 1943, p. 191.

32. D. R. Uhlmann, B. Chalmers and K. A. Jackson, "Interaction Between Particles and a Solid-Liquid Interface", Jl. Appl. Phys., Vol. 35, 1964, pp. 2986-1993.

33. E. T. Turkdogan, "Cause and Effects of Deoxidation Occuring During Cooling and Solidification of Steel", Trans. Met. Soc. AIME, 1965, p. 2100.

34. E. T. Turkdogan, "Nucleation, Growth, and Flotation of Oxide Inclusions in Liquid Steel", Jl. Iron and Steel Inst., Vol. 914, 1966.

35. T. Z. Kattamis, J. C. Coughlin and M. C. Flemings, "Influence of Coarsening on Dendrite Arm Spacing of Aluminum-Copper", Trans. AIME, Vol. 239, 1967, p. 1504.

36. J. W. Cahn and J. E. Hilliard, "An Evaluation of Procedures in Quantitative Metallography for Volume Fraction Analysis", Trans. AIME, Vol. 221, April 1961.

37. H. P. Brody and M. C. Flemings, "Solute Redistribution in Dendritic Solidification", Trans. AIME, Vol. 236, 1966, pp. 615-624.

38. G. N. Greenwood, "The Growth of Dispersed Particles in Solutions", Acta. Met., Vol. 4, 1956, pp. 243-248.

39. I. M. Lifshitz and V. V. Slyozov, "Kinetics of Diffuse Decomposition of Supersaturated Solid Solution", J. Experimental Theoretical Physics (USSR), Vol. 35, 1958, pp. 479-492.

40. E. H. Fontana and W. A. Plummer, "A Study of Viscosity-Temperature Relationships in the GeO_2-SiO_2 Systems", Phys. and Chem. of Glass, Vol. 7, No. 4, 1966.

TABLE 1

Critical Velocities for Particle-Organic Matrix Systems in Order of Increasing Critical Velocity

orthoterphenyl		salol		thymol	
particle	v_c (μ/sec)	particle	v_c (μ/sec)	particle	v_c (μ/sec)
AgI	not pushed	AgI	not pushed	Fe_2O_2	2
Graphite	0.3	Graphite	not pushed	Sn	4
MgO	0.5	Silt	0.7	AgI	6
Silt	0.7	Si	0.8	Zn	6
Si	0.8	Sn	1	MgO	8
Sn	1	Diamond, 0-2	2	Ni	8
Diamond, 0-2	1.3	Diamond, 3-5	2.1	Diamond, 3-5	9
Diamond, 3-5	1.4	Ni	2.3	Si	10
Ni	2	Fe_2O_3	2.5	Graphite	12
Fe_2O_3	2.5	MgO	3	Silt	16
Zn	2.5	Zn	7		

TABLE 2

Dendrite Arm Spacing of Master Alloy and Isothermally Coarsened Specimens

sample	dendrite arm spacings, vert. sect. (microns)	dendrite arm spacings, horiz. sect. (microns)	average
Master	18	18	18
1275°C - 1/2 hour	29	31	30
1275°C - 2 hours	33	34	34
1275°C - 4 hours	64	55	60
1400°C - 1/2 hour	38	41	40
1400°C - 2 hours	88	75	81

Note: Solidification time of the master alloy was approximately 7 minutes.

TABLE 3

Chemical Analysis

sample	Cu (wt.%)	Si (wt.%)	SiO_2 (wt.%)
Master	50.6	.017	.027
1275°C - 1/2 hour	-	.016	.030
1275°C - 4 hours	-	.023	.033
1400°C - 1/2 hour	50.1	.015	.029
1400°C - 2 hours	51.5	.021	.028

TABLE 4

Mean Apparent Diameter of Inclusions
Trapped in Iron Dendrites

specimen	number trapped inclusions	mean dia. (microns)
Master	102	3.0
1/2 hour - 1400°C	118	2.8
2 hours - 1400°C	102	3.0

TABLE 5

Calculation of Critical Time for Dendrite Coarsening

$$t_c = \left(\frac{1}{\sigma}\right) \frac{HC_L(1 - k)md^3}{D\,T}$$

at 1400°C	at 1275°C
$\sigma = 4.7 \times 10^{-6}$ cal/cm^2	$\sigma = 4.7 \times 10^{6}$
H = -507 cal/cc	H = -507
k = .103	k = .087
m = -3.70 °K/% Cu	m = -23
d = 30×10^{-4} cm	d = 30×10^{-4}
T = 1673°K	T = 1548°K
D = 5×10^{-5} cm^2/sec	D = 5×10^{5}
C_L = 78%	C_L = 92%

$t_c(1400) = 9.03 \times 10^3$ sec

$t_c(1275) = 7.23 \times 10^4$

$$\frac{t_c(1275)}{t_c(1400)} = \frac{72.3 \times 10^3}{9.0^3 \times 10^3} = 8.04$$

TABLE 6

Critical Velocity for Trapping of Inclusions

$$v_c = 1/2(\eta + 1)(La_o V_o D/kTR^2)$$

L	=	4.5×10^2 cal/cm^3	D	=	10^{-5} cm/sec^2
η	=	5	k	=	33×10^{-24} cal/°K
V_o	=	27×10^{-8} cm^3	T	=	1700°K
a_o	=	3×10^{-8} cm	R	=	1.5×10^{-4} cm

v_c = 9.7×10^{-4} cm/sec = minimum growth rate at which 3μ inclusions will be trapped by the growing iron dendrites.

TABLE 7

Minimum Time for Complete Coalescence of Two Spheres

$$t_c = \frac{r\eta}{\sigma}$$

t_c = time

r = radius = 1.5 microns

η = viscosity 3×10^{10} poise (ref. 40)

σ = interfacial energy = 1000 ergs/cm^2 (ref. 22)

$$t_c = \frac{1.5 \times 10^{-4}(3 \times 10^{10})}{10^3} = 4.5 \times 10^3 \text{ sec.}$$

t_c = 4500 sec.

TABLE 8

Diffusional Coarsening Calculation

Assume SiO_2 spheres of initial mean diameter of 2.8 microns. Calculate diameter d, after holding in liquid at 1400°C for 1/2 and 2 hours.

$$r^3_{(t)} = r^3_{(0)} + \alpha k t \quad \text{(ref. 5,35,39)}$$

$$\alpha = \frac{4}{9}, \text{ a geometric constant}$$

$$k = \frac{2\sigma V_m C_o D}{RT(C_p - C_o)}$$

where

r = radius

σ = surface energy = 1000 dynes/cm^2

V_m = molar volume of diffusing $\underline{O}$ = 13 cc/mol

C_o = concentration of $\underline{O}$ = 100 ppm = 7×10^{-4} g/cc

C_p = concentration of $\underline{O}$ in SiO_2 = 1.2 g/cc

D = diffusivity of $\underline{O}$ = 5×10^{-5} cm^2/sec

R = universal gas constant = 8.31×10^7 dynes/cm^2mole

T = 1673°K

Table 8 (cont'd)

$$r^3 = 2.74 \times 10^{-12} + 5.67 \times 10^{-15}(t)$$

$$r^3_{(1/2)} = 7.2 \times 10^{-12}$$

$$r_{(1/2)} = 1.93 \times 10^{-4} \text{ cm}$$

$$d_{(1/2)} = 3.86 \text{ microns}$$

Similarly, $d_{(2)} = 5.5$ microns

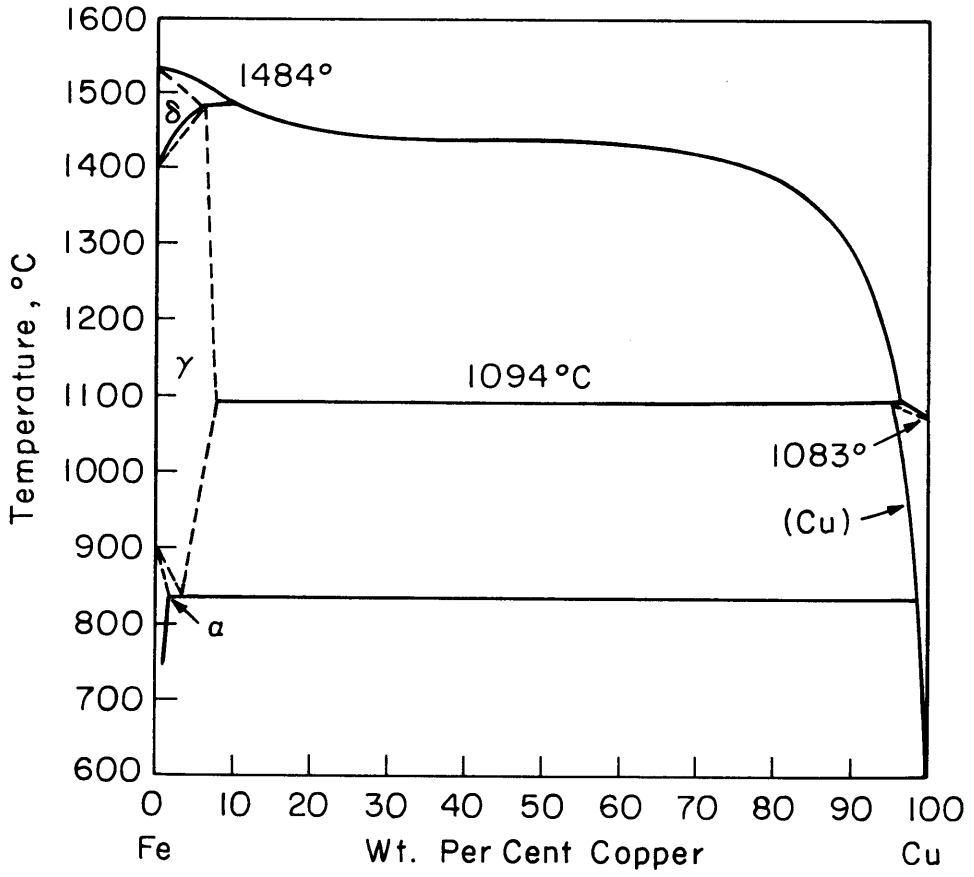

Figure 1. Iron-copper phase diagram.
(ASM Metals Handbook 1948 ed.)

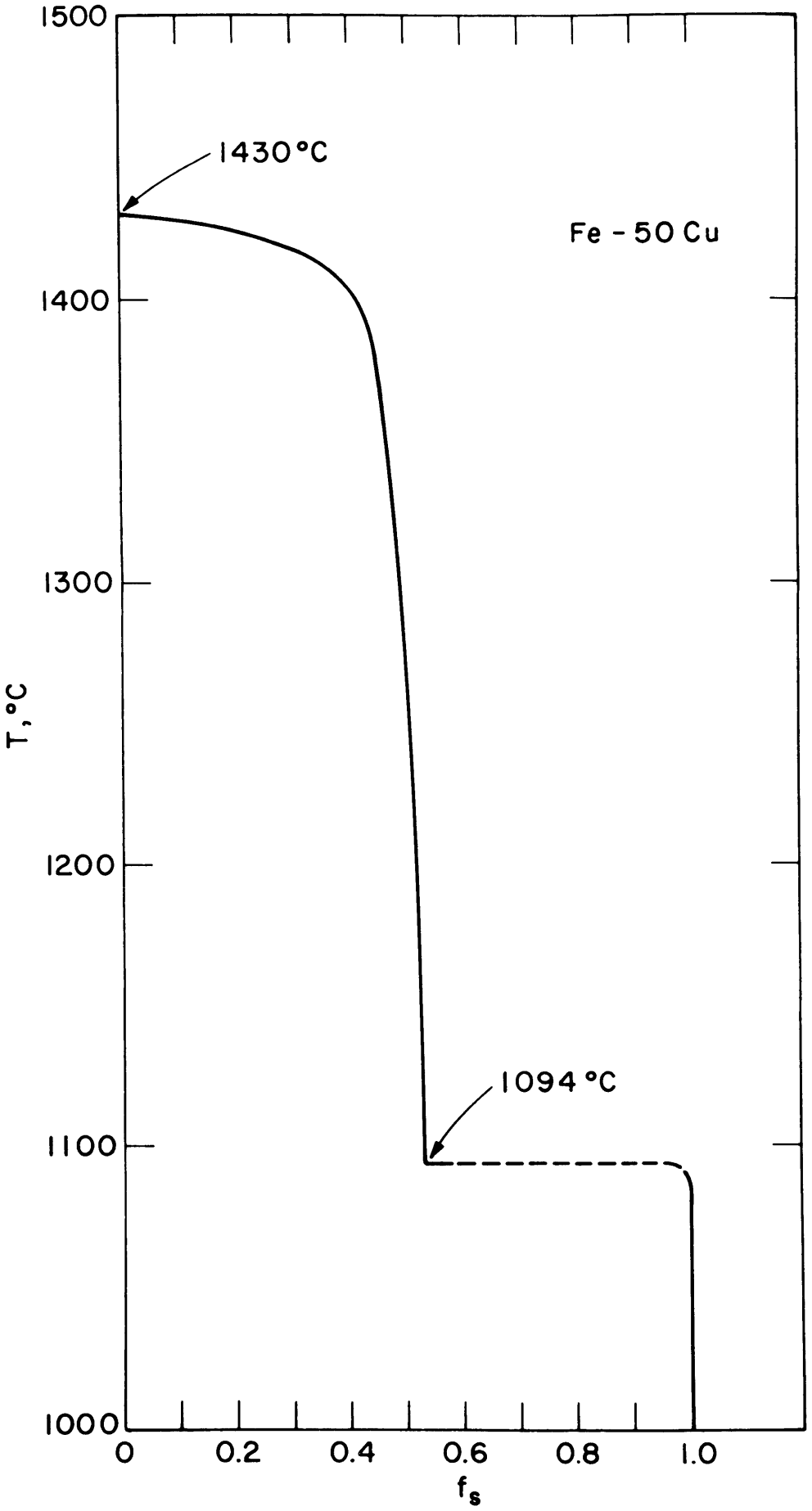

Figure 2. Fraction solid vs. temperature for Fe-50%Cu

vertical section

horizontal section

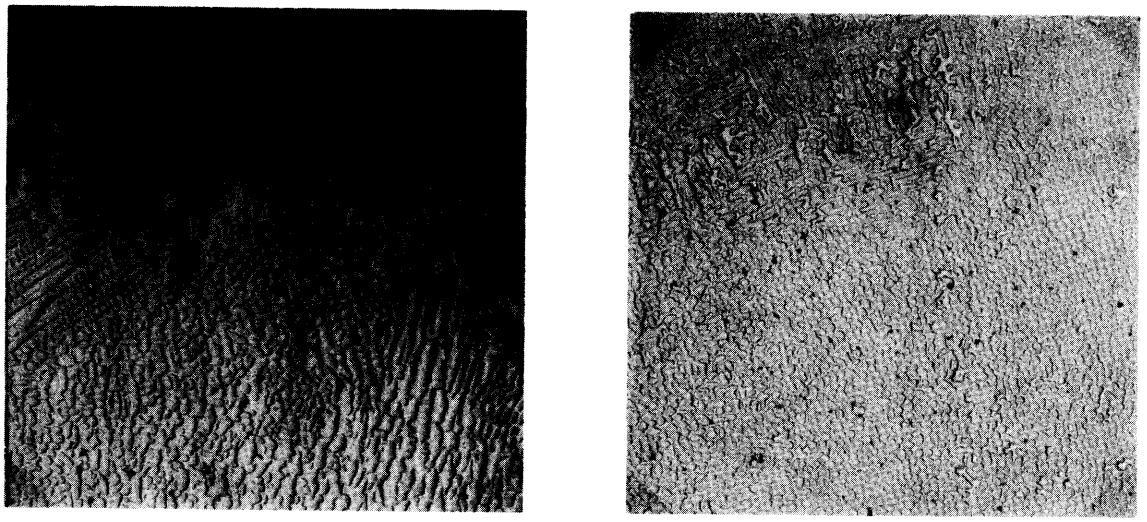

55X

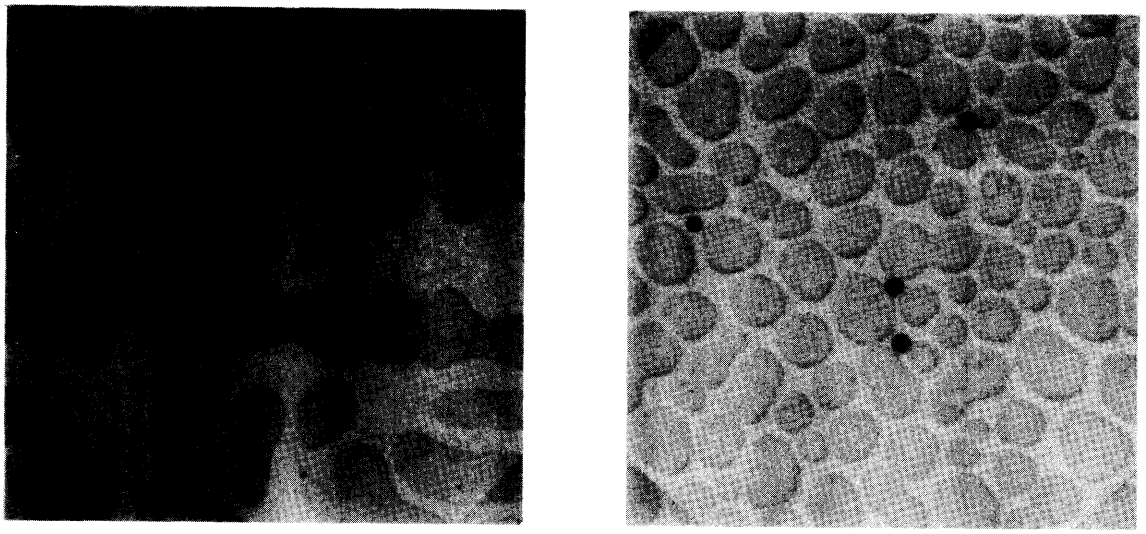

500X

Figure 3. Fe-50% Cu master (as cast)

vertical section

horizontal section

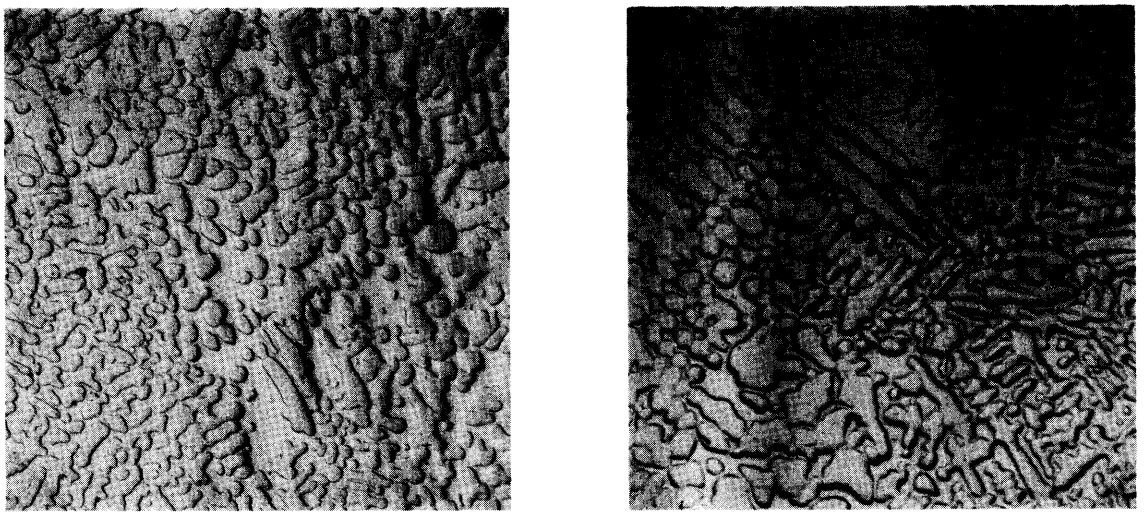

55X

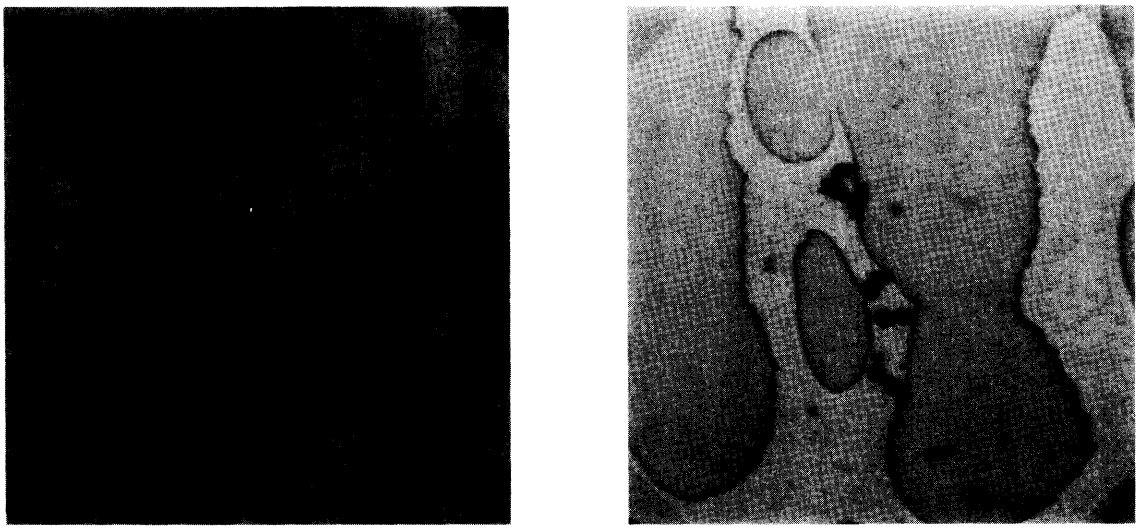

500X

Figure 4. After isothermal holding ½ hour at 1275°C

vertical section

horizontal section

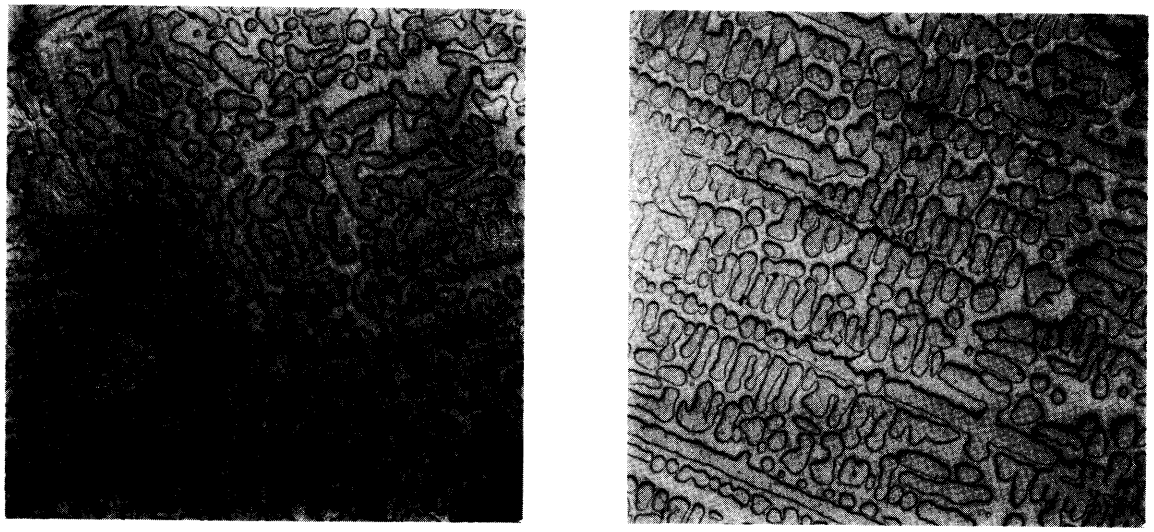

55X

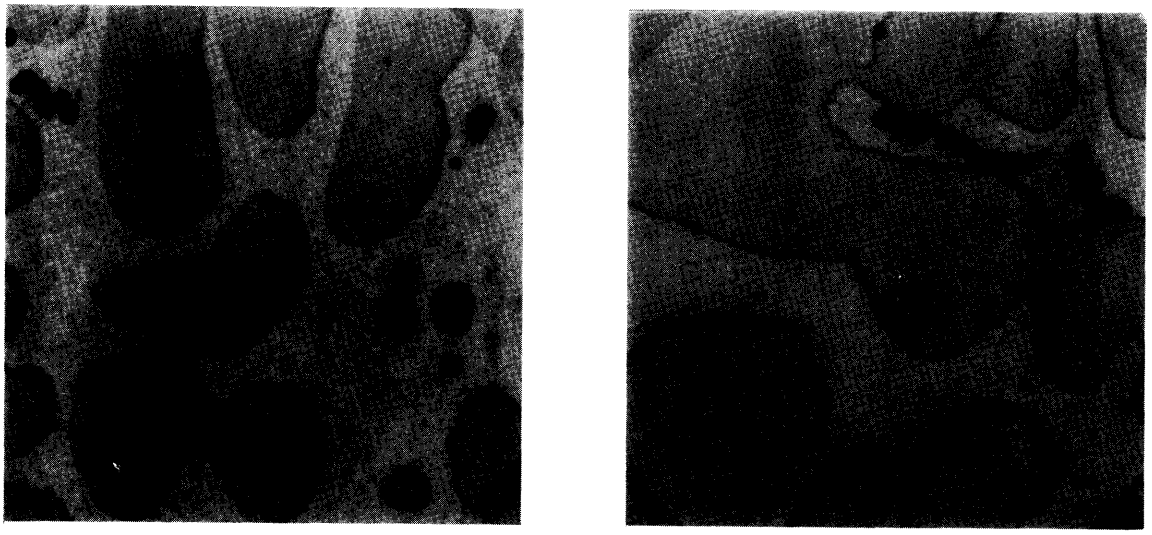

500X

Figure 5. After isothermal holding 2 hours at 1275^{o}C

vertical section

horizontal section

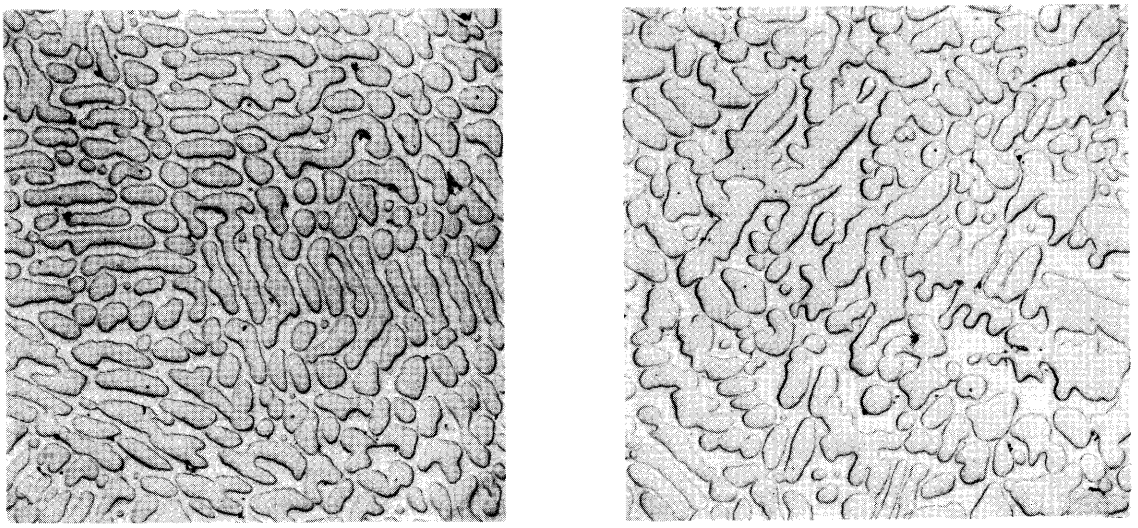

55X

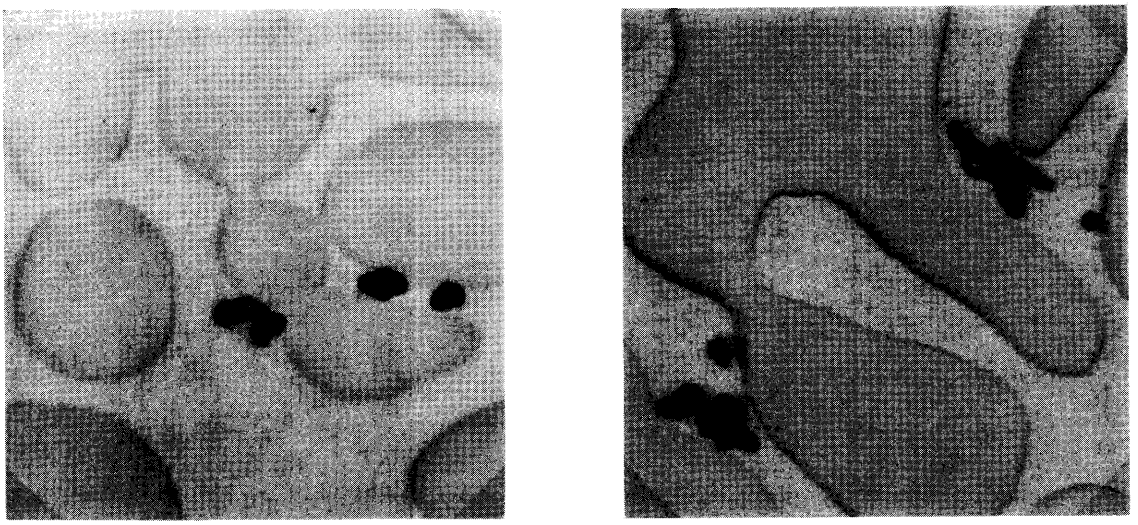

500X

Figure 6. After isothermal holding 4 hours at 1275°C

vertical section

horizontal section

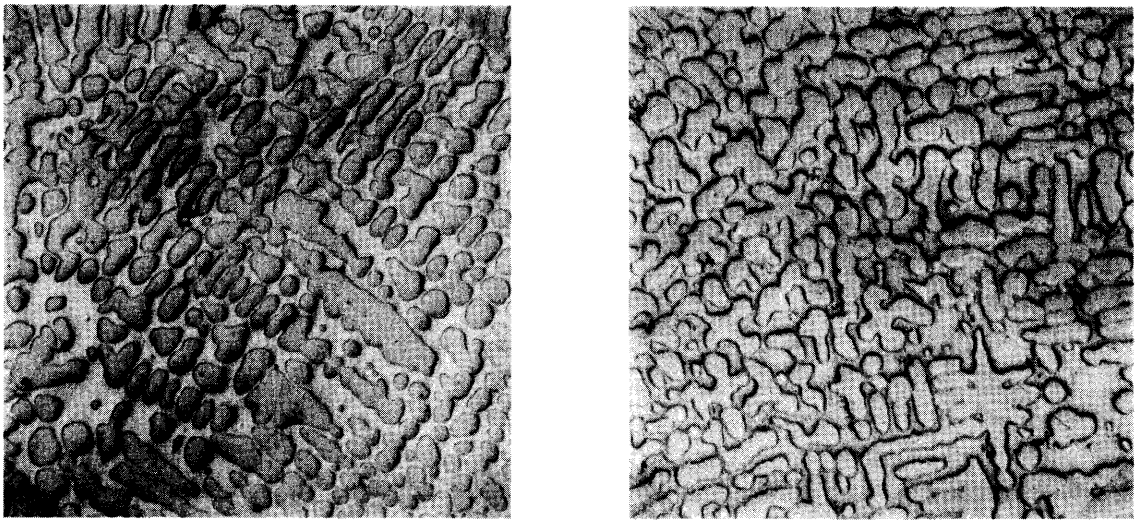

55X

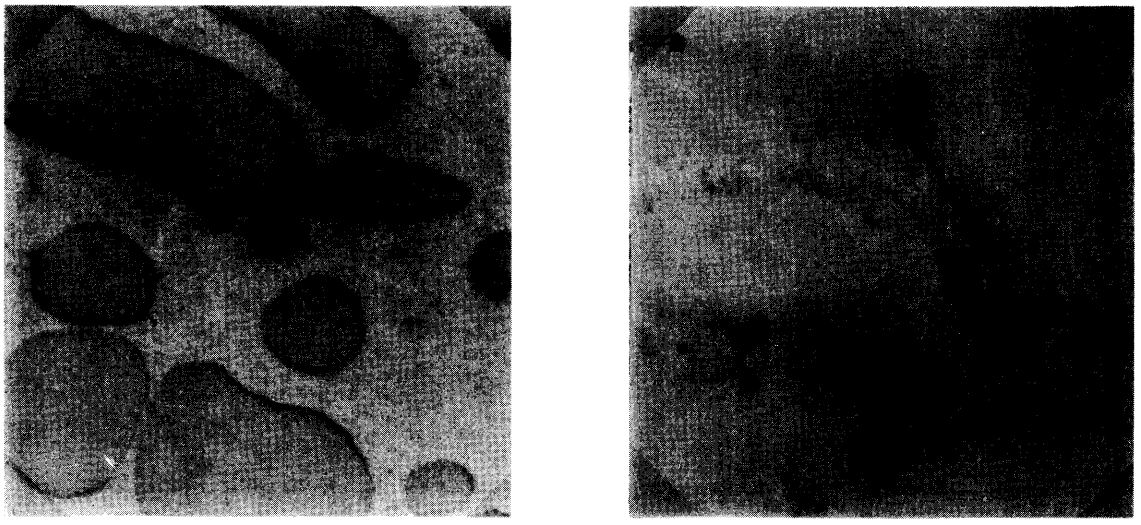

500X

Figure 7. After isothermal holding ½ hour at 1400°C

vertical section

horizontal section

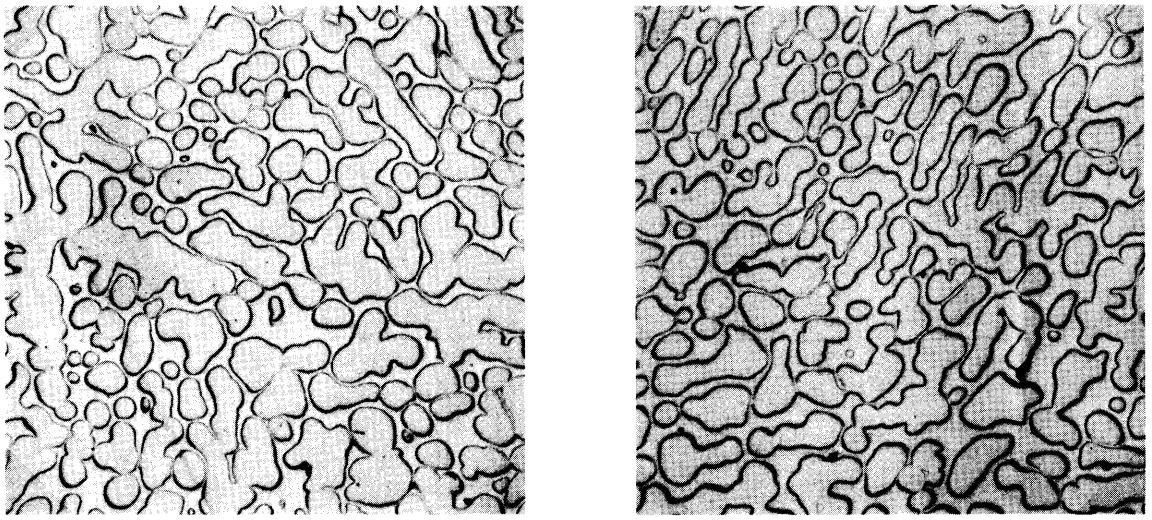

55X

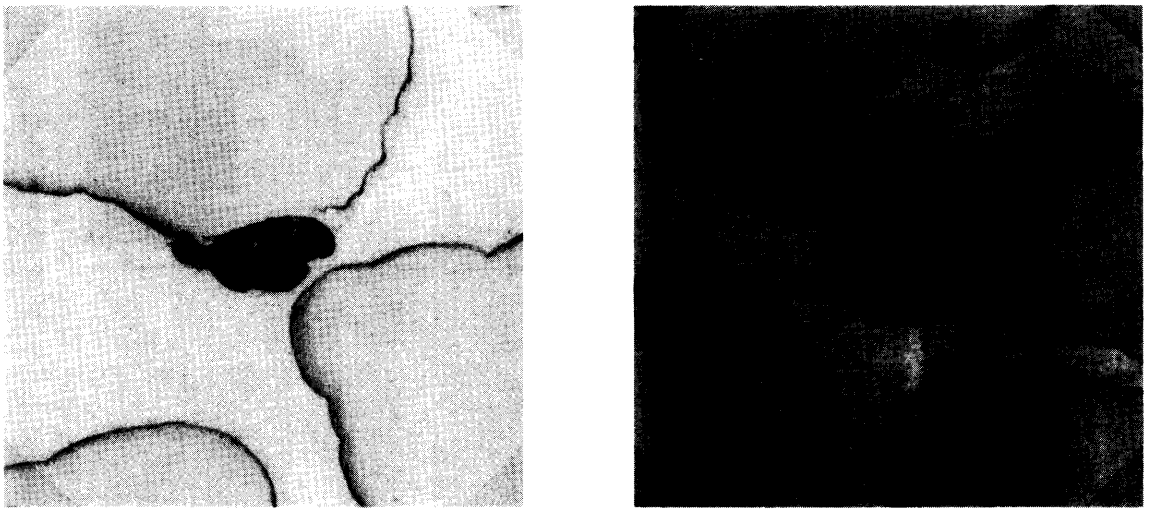

500X

Figure 8. After isothermal holding 2 hours at 1400°C

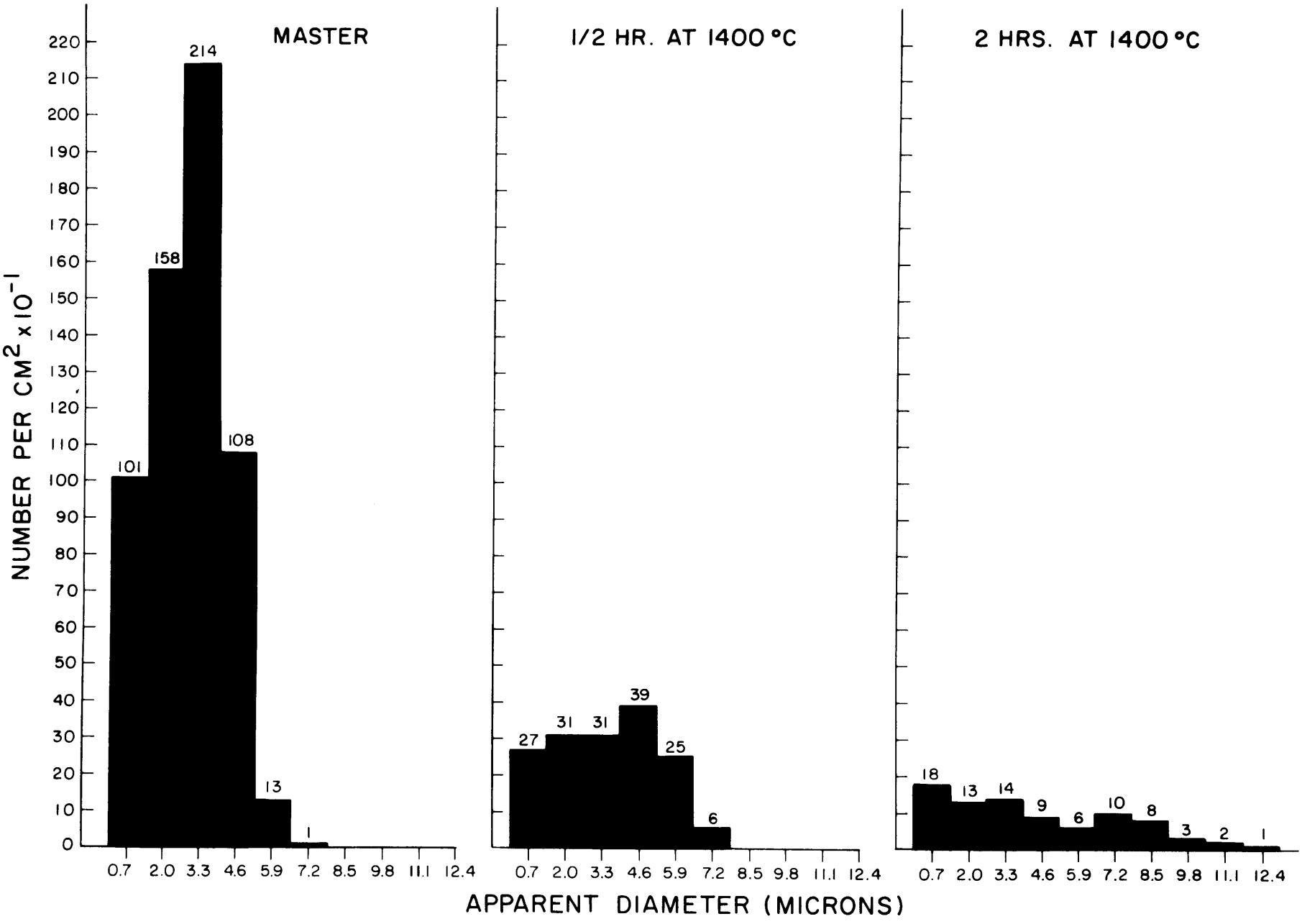

Figure 9. Size distribution of single membered inclusions in second phase.

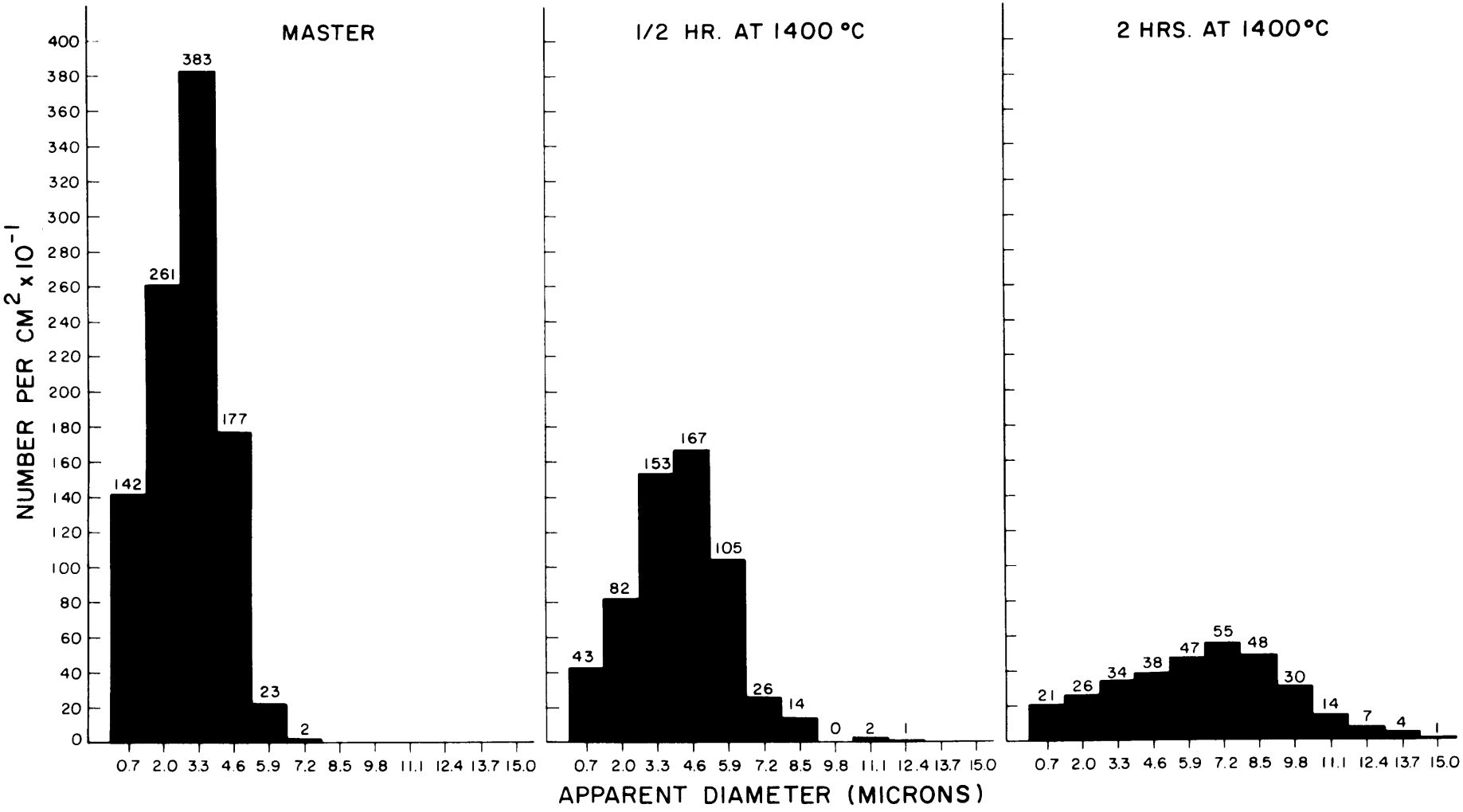

Figure 10. Size distribution of all inclusion members in second phase.

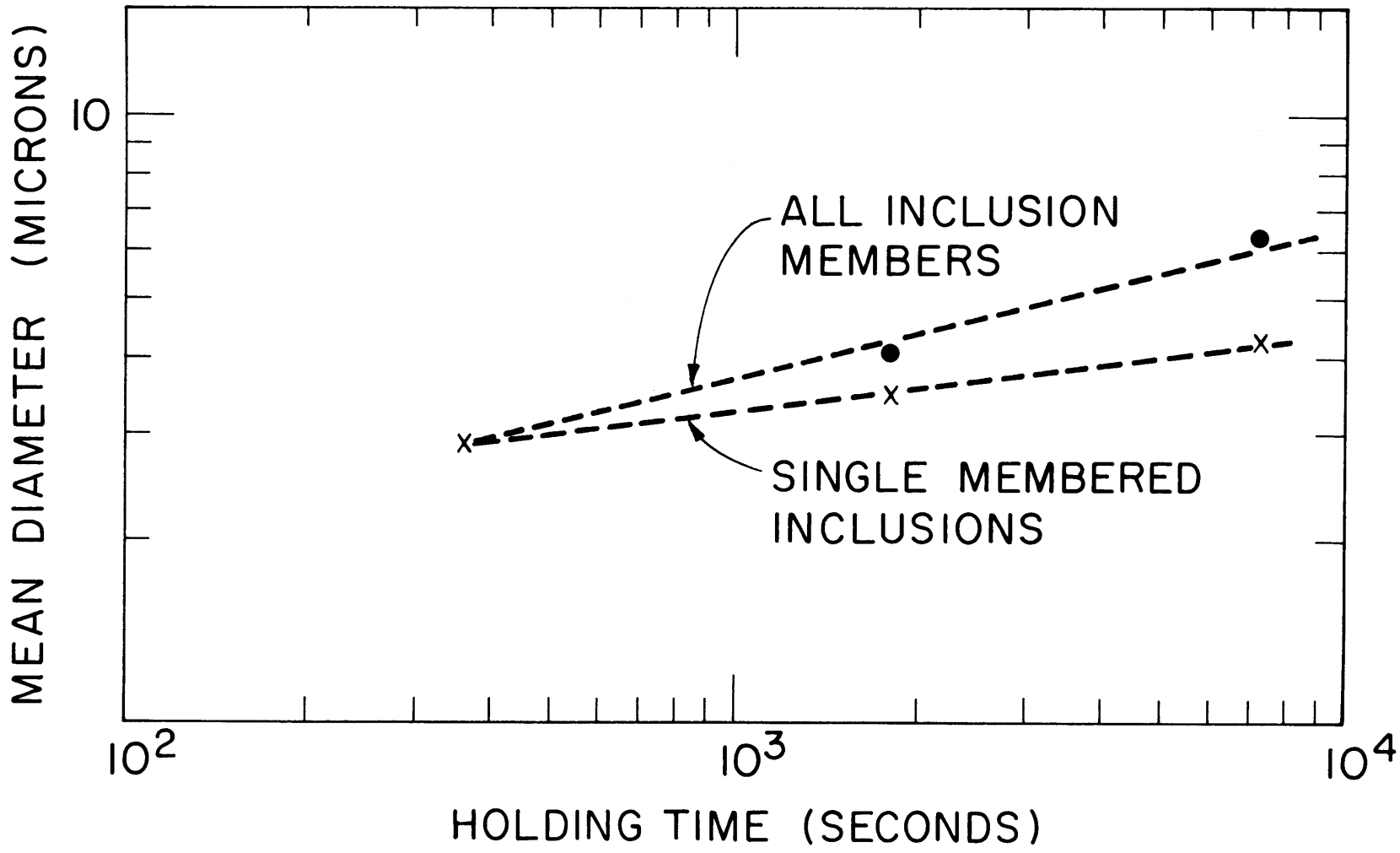

Figure 11. Mean apparent inclusion member diameter vs. time at 1400°C.

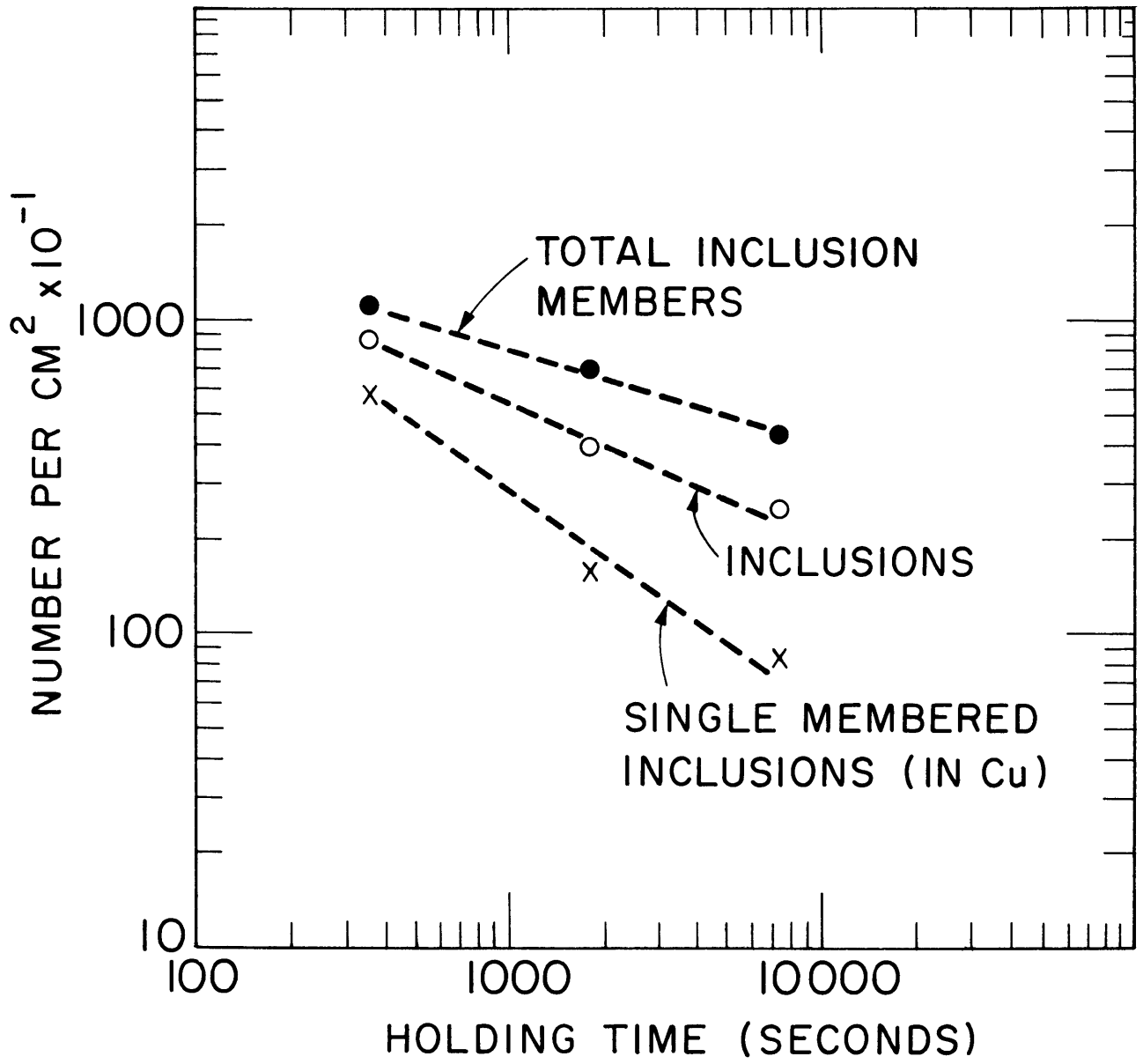

Figure 12. Number of single membered inclusions, inclusion members, and inclusions, per unit area vs. time at 1400°C.

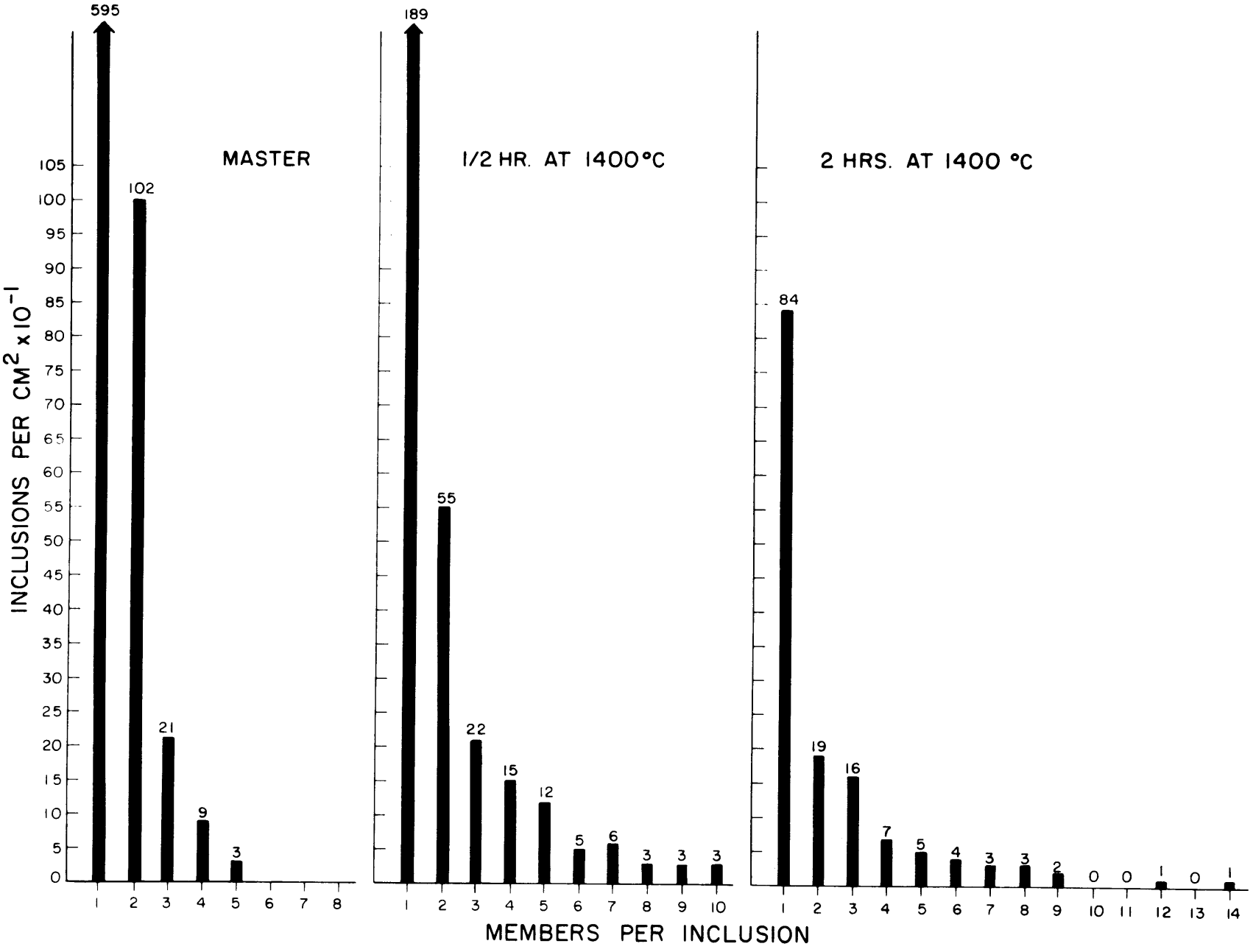

Figure 13. Members per inclusion before and after holding at 1400°C.

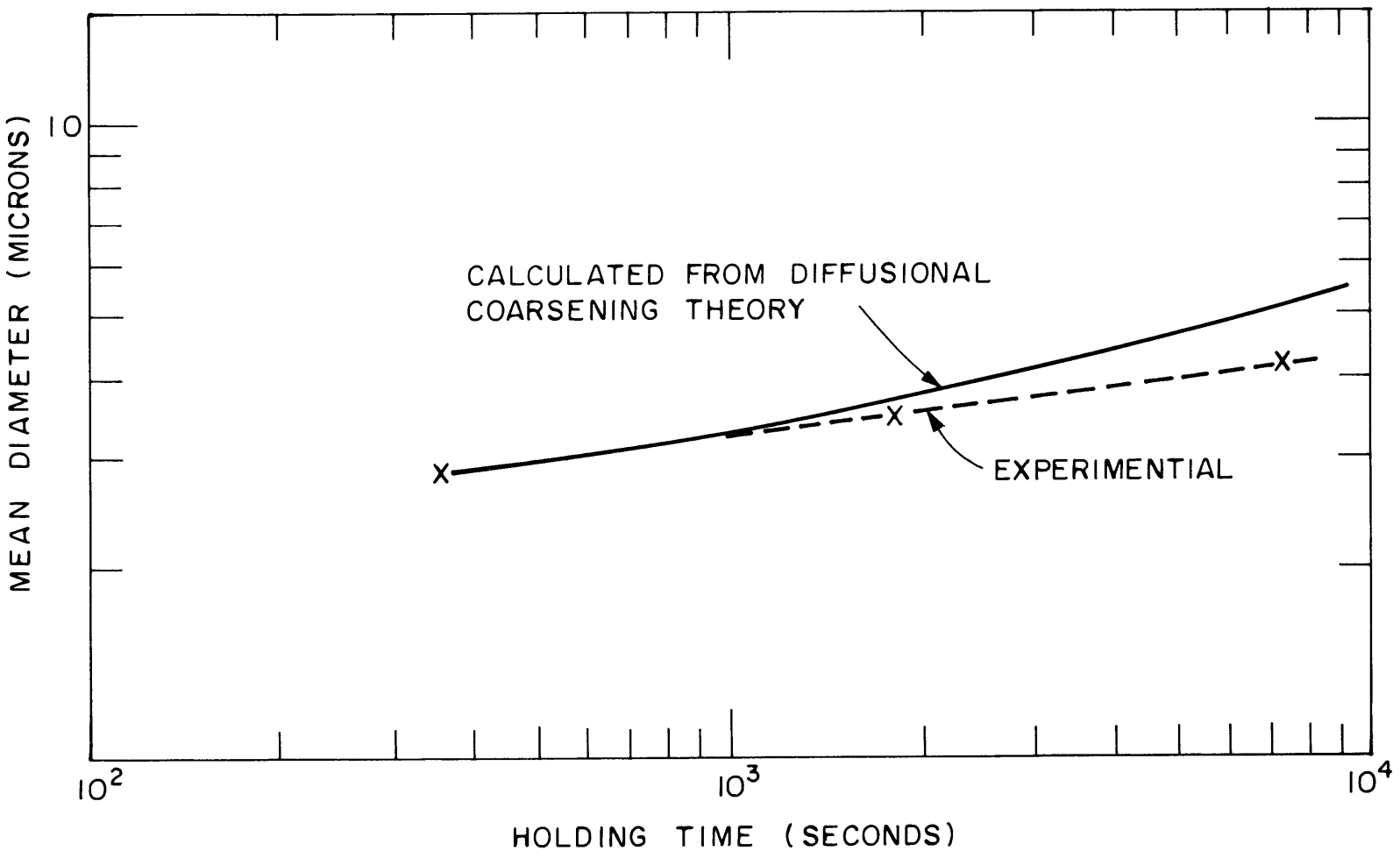

Figure 14. Apparent and theoretical mean diameter of single membered inclusions isothermally held at 1400°C.

Chapter 3: LEVITATION MELTING AND CASTING

Introduction

Extensive work has been done during the last year modifying and extending the capabilities of an existing levitation melting unit. This work has been primarily to (1) improve the vacuum system and purity of cooling gases employed, (2) incorporate ability to make chill plate castings and to liquid quench the molten droplets, and (3) permit making up to five separate runs without breaking vacuum. This work is now complete and capabilities of the apparatus include the following:

1. Ferrous metals or alloys can be levitation melted in amounts up to about 3 grams in vacuum or controlled atmosphere. A wide variety of other metals can also be so melted.

2. Samples can be held molten or partially molten for long periods (e.g., in excess of 1/2 hour). Larger superheats can be obtained (in excess of 600°C). Large undercoolings can be achieved (as much as 300°C under the melting point).

3. Alloying can be accomplished by simultaneously melting two or more charge materials (while levitated) or by reaction of the charge with a controlled atmosphere. Alternately, the charge can be pre-alloyed.

4. Up to five separate melting and casting runs can be made without opening the apparatus to the atmosphere.

5. The metal charge can be solidified by (a) slow controlled cooling in the levitation coil, (b) liquid quenching, (c) casting in thin section ingot molds, and (d) "splat cooling".

6. Interrupted solidification experimentals can be conducted by, for example, partially solidifying the sample (slowly) in the coil and then rapidly solidifying the remainder by liquid quenching or splat cooling.

The basic levitation melter employed has been previously described[1]; it is based work of Comenetz and others[2-6]. The "hammer and anvil" splat cooling device has also been previously described[1]. The propulsion of the hammer is electromagnetic. A large current is released for a short time through a "pancake" coil adjacent to a driving disc. The driving disc is then repulsed from the coil with a force that may be calculated from magnetodynamic principles.[7-8]. In the splatter used in the current work, the force achievable is 2200 to 6600 pounds; resulting platen velocity is 1000 to 3000 cm/sec. (33 to 100 ft/sec.)*. Remaining portions of the apparatus have

---

* In an auxiliary hammer and anvil device not currently being used, forces have been obtained up to 12,000 pounds with resulting velocities up to 9000 cm/sec. (296 ft/sec.).

been constructed in the course of this research and are described in the following sections.

Work during the current contract year has been primarily on modification and improvement of the apparatus, as described above, and this report will deal almost exclusively with that work. In addition, the following experimental program is in progress; some preliminary results are given in a later section of this report.

1. A comprehensive study is underway on effect of undercooling, superheating, and especially on effect of cooling rate on inclusion formation and growth. Current work is primarily on the Fe-Si-O system; this system has the advantages that the phase diagram is simple and well known. Preliminary results indicate that formation of silica inclusions is completely suppressed at sufficiently rapid cooling rate.

2. Structure and mechanical properties of undercooled and/or rapidly solidified AISI 4330 are being studied. Procedures have been developed to permit obtaining test bars from the plates, and hopefully, from the splats. Study is planned of relation of properties to structure, with emphasis on inclusions and macrosegregation.

3. Work is continuing on general relations of structure to undercooling and cooling rate. For example, the equipment readily permits correlation of dendrite arm spacing with cooling rate (since variation in cooling rate of over

6 orders of magnitude is feasible). Extensive data have been obtained in this way for Fe-26% Ni, AISI 4340, and Fe-50% Cu.

Apparatus - General

Figure 1 is an overall sketch of the levitation melting and quenching apparatus, and Figure 2 (top) a photograph of the apparatus, including power supply. Descriptions are given below of the melting, temperature measuring, atmosphere controlling, gas quenching, liquid quenching, chill casting, and splat quenching systems. Figures 3 to 7 show details of some of these systems.

Levitation System

The levitation melter constructed for this work was designed to be operated with a 10 KW, 400 K.C. Lepel High Frequency Generator. This power source is capable of an output of approximately 300 amperes into a suitable impedance load, but is limited to less than this into the relatively low inductance levitation coil. Figure 3 shows a levitation coil of the type presently in use; it is made from 1/8 inch diameter, thin wall copper tubing.

The most practical technique for temperature control during levitation involves flowing a stream of cooling gas over the levitated charge. This is readily done by winding a levitation coil, such as the one on the left in Figure 3, around a

Vycor tube of large enough diameter to contain the specimen, and then flowing cooling gas vertically up the tube.

To obtain good "matching" to the generator and to increase the circulating current in the coil, a capacitor bank (Lepel CT-25-4) was inserted into the output circuit in parallel with the levitation coil. The coil and the capacitor bank form a resonant circuit, having a large circulating current, measured to be over 650 amperes at full power. Physically, the capacitor is located close to the levitation coil and they are connected using co-axial power leads to minimize power losses. A schematic diagram of the external electrical circuit is given in Figure 4.

The enclosure containing charges and ingot molds is shown schematically in Figure 1. Up to five charges are placed in each charge container prior to evacuating the system. The charge container is of boron nitride to prevent its being heated when raised into the levitation coil. Charging is accomplished by first rotating the turntable into position so one of the five charges is directly beneath the vertical glass tube. Next, the charge and charge container are raised up into the levitation coil by pushing on a vertical pushrod which extends out the bottom of the box. This pushrod also serves as a "charge exit port" for splatting and is so named in the sketch. An "O" ring seal between the pushrod and enclosure allows the lateral motion while maintaining vacuum or slight positive pressure in the enclosure.

The turntable also contains up to five ingot molds. To cast one of these, it is simply rotated under the coil while the droplet is levitated. The power is turned off and metal dropped into the plate. To "splat" a sample, one of the locations for an ingot mold is left vacant, and this location placed under the levitated drop. When the levitation power is turned off, the droplet passes through the hole, down the hollow "pushrod-charge exit port", and through a plastic sheet sealed at the base of the exit port. This sheet plastic seal covers a 5/8" hole; vacuum or positive pressure is again maintained by an "O" ring seal. The seal is "Saran Wrap" (polyvinylidene chloride copolymerized with polyvinyl chloride); it is sufficiently strong to resist atmospheric pressure while the enclosure is fully evacuated, but rapidly melts as the falling hot drop approaches it.

The temperature of the levitated droplet is monitored using a Milletron Two-Color Pyrometer, Model TSA. Its accuracy varies with the material whose temperature is being measured, but has been found in this work (and with this system) to be accurate on absolute measurements on liquid iron and steel to within $\pm$ 20°C and to within $\pm$ 10°C relative to the measured melting point. Output is read on a meter in the control unit, and may be recorded on an external chart recorder. A schematic diagram of the temperature measuring system is shown in Figure 5. Sighting of the optical pyrometer is done from the top of the levitation coil through a right

angle prism and a flat glass disc glued to the top of the glass tube surrounding the specimen. The disc is well above the levitation coil (8") to prevent deposition on it of vapors from the levitated charge.

Controlled Atmosphere and Gas Cooling System

A schematic diagram of the controlled atmosphere and gas cooling system is shown in Figure 6. Evacuation of the system is accomplished by means of mechanical and diffusion pumps, acting through a 1-3/8" hole in the bottom of the enclosure containing the charges and ingot molds. A thermocouple vacuum gauge is permanently mounted on the enclosure, and a vacuum ion gauge may be attached to one of the two standard vacuum fittings.

The desired gas atmosphere (or combination of gases) is admitted through copper tubing to flow rate control and solenoid-operated check valves. Ability to admit a large and variable flow rate (up to 250 cubic feet per hour), to the system permits temperature control of the levitated charge. The cooling gas passes up the 5/8" I.D. Vycor tube surrounding the levitated specimen and exits through a vacuum released valve. This valve acts as a vacuum seal when the system is evacuated. All connections in the gas flow system are 3/8" copper tubing to prevent gas contamination.

Quenching Mechanisms

The various ways summarized below of solidifying the samples permit obtaining cooling rates of the orders of: 1 - 10°C/sec. for gas quenching; 30 - 200°C/sec. for liquid quenching, to 10^3 - 10^4°C/sec. for chill casting, to 10^5 - 10^6°C/sec. for splat cooling.

With sufficiently high flow rates of hydrogen or helium it is possible to solidify a molten levitated charge. At the relatively slow rates of cooling normally involved, the cooling rate may be measured from the chart recorder of the optical pyrometer. This cooling rate simulates those observed in relatively large castings. As noted previously, quenching into liquid is achieved by placing a liquid quench tank under the charge exit port in place of the splat cooler, and dropping the charge through the plastic seal.

To achieve still higher cooling rates, copper molds with plate-shaped mold cavities of varying thickness are inserted in the turntable in the enclosure in Figure 1. These copper molds are one inch diameter split cylinders with a wedge or conical shaped riser section above the plate cavity and 1/64" vent holes below the plate cavity to aid in mold filling. Plate thicknesses are .03", .05", and .08". For best mold filling, molds are polished each time and minimum superheat of 100°C employed.

An important feature of the arrangement for "splatting" shown in Figure 1 is that the rather delicate levitation melting device and its attachments are physically separate from the necessarily violent clapper (clapping velocities are up to 200 miles per hour).

The drive mechanism for the "hammer and anvil" type splat cooler shown in Figure 7 consists of a driving coil and capacitor energy storage bank, a power supply to charge the capacitor bank, droplet sensing equipment, and spark gap switch with associated trigger circuitry. The capacitor bank and associated power supply are manufactured by EG & G International, Inc. The capacitor bank consists of two separate but equivalent units, Models 524 and 233, each containing capacitors totalling 320 microfarads and having a storage capacity of 2500 joules at 4.0 KV. These two units are connected in parallel, and to the power supply, Model 522, which has a 0 - 4.0 KV adjustable voltage output. The power supply unit also contains circuitry to provide a voltage pulse output to trigger the spark gap, upon an external contact closure.

The droplet sensor is a Knight photoelectronic relay (kit). A CdSe photocell is located close to the clapper platens, in the line of sight of fall of the molten droplet. When activated by a falling droplet, a relay contact is closed, and through connection with the power supply trigger circuit, provides a voltage pulse to trigger the spark gap. The spark

gap unit consists of an EG & G experimental "rail-type" spark gap and an EG & G trigger transformer. The pulse from the power supply is transformed to a much higher voltage, which ionizes the spark gap and causes electrical breakdown, rendering the spark gap conducting, and discharging the capacitor bank into the driving coil.

Upon sensing a falling droplet, the spark gap is triggered and the energy stored in the capacitor bank is released into the driving coil. The large current pulse through the driving coil, associated with the capacitor discharge, creates an intense magnetic field around the coil which in turn induces eddy currents in the aluminum driving disc. The eddy currents cause another magnetic field out of phase with the first. Thus, the driving plate is repelled from the coil at high speed. The capacitor discharge primary pulse lasts approximately 0.1 - 0.2 milliseconds; the moving elements are accelerated to maximum speed during this time.

Operation of the splat cooler and associated equipment is briefly as follows. The clapper platens are cleaned and the moving platen assembly is set in the open position with driving plate against the driving coil. The droplet sensing photocell is inserted into position in the side of the protective cover and the cover is placed over the clapper. After the induction power is turned on and the specimen levitated, the clapper power supply is energized to charge the capacitor bank to the desired voltage. Specimen temperature is manipulated by

changing gases or gas flow rate. When proper conditions have been attained, the induction power is switched off. The specimen falls and is sensed by the photocell which triggers the capacitor discharge. The moving platen smashes the falling specimen against the back platen to form a splat. Total elapsed time between sensing the specimen by the photocell and splatting is about five milliseconds.

Structures

Some preliminary results are summarized herein to demonstrate the range of structures obtainable using the apparatus described above. Structures are presented for two commercial steels (440C and 4330) and for a specially prepared Fe-Si-O alloy. Commercial 440C and 4330 alloys were solidified using the gas quenching, liquid quenching, chill casting and splat cooling techniques. Helium was used to solidify the molten charge during levitation. Liquid quenching was accomplished by dropping the charge from the levitation coil through the charge exit port into an oil bath. Small plates of 0.05" thickness were chill cast in the copper molds in the enclosure. Splat cooled castings of 100 microns thickness were made using a platen velocity of 1000 cm/sec.

The different structures obtained in these two alloys are shown in Figures 8 and 9; dendrite arm spacing varies from about 50 microns in the slowest solidified samples to less than 1 micron in the splats.

The iron-silicon-oxygen alloy was prepared in the vacuum induction furnace by adding 0.05 weight per cent silicon to Ferrovac "E" iron and equilibrating with a silica crucible for 20 minutes at 1550°C. Two gram pieces of this master alloy were then remelted in the levitation furnace. After holding the iron-silicon-oxygen alloy at 1600°C for 30 seconds to insure dissolution of the silica inclusions, four specimens were cast as were the commercial alloys (i.e., by gas quenching, oil quenching, plate casting and splat cooling).

Structures of the starting alloy and two of the castings are shown in Figure 10. The slowly solidified starting alloy had numerous large inclusions, the gas cooled casting somewhat finer inclusions, and the oil quenched specimen still finer inclusions. Inclusions in the plate castings were very much finer than those in the oil quenched specimen. No inclusions at all have yet been found in the splatted specimen. Electron microscopic study of similar specimens is now underway.

Summary

A levitation melting, undercooling, and splat cooling device has been modified to permit greater flexibility of operation and to incorporate ability to make chill plate castings (for study of mechanical properties as well as for structure). Dendrite arm spacing of commercial steel alloy castings made in this apparatus varies from about 50 microns

for gas cooled specimens to less than 1 micron for splat cooled specimens. In work on Fe-Si-O alloy, no optically visible inclusions have been found in splat cooled samples.

References

1. R. W. Strachan, "A Technique for Levitation Melting, Undercooling, and Splat Cooling of Metals and Alloys", Ph.D. Thesis, Department of Metallurgy, M.I.T., 1967.

2. E. Okress, D. Wroughton, G. Comenetz, P. Brace, and J. Kelly, "Electromagnetic Levitation of Solid and Molten Metals", Jl. Appl. Phys., Vol. 23, 1952, pp. 545-552.

3. E. Fromm and H. Jehn, "Electromagnetic Forces and Power Absorption in Levitation Melting", Jl. Appl. Phys., Vol. 16, 1965, pp. 653-663.

4. W. A. Peifer, "Levitation Melting....A Survey of the State of the Art", Jl. of Metals, May 1965, pp. 487-493.

5. B. Harris and A. E. Jenkins, "Controlled Atmosphere Levitation System", Jl. of Sci. Inst., Vol. 36, 1959, pp. 238-240.

6. S. Y. Shiraishi and R. G. Ward, "The Density of Nickel in the Superheated and Supercooled Liquid States", Can. Met. Quarterly, Vol. 3, 1964, pp. 117-122.

7. D. H. Birdsall, F. C. Ford, H. P. Furth, and R. E. Riley, "Magnetic Forming", American Machinist, Vol. 105, 20 March 1961, pp. 117-121.

8. H. P. Furth, "Magnetic Pressure", International Sci. and Tech., No. 57, September 1966, pp. 32-40.

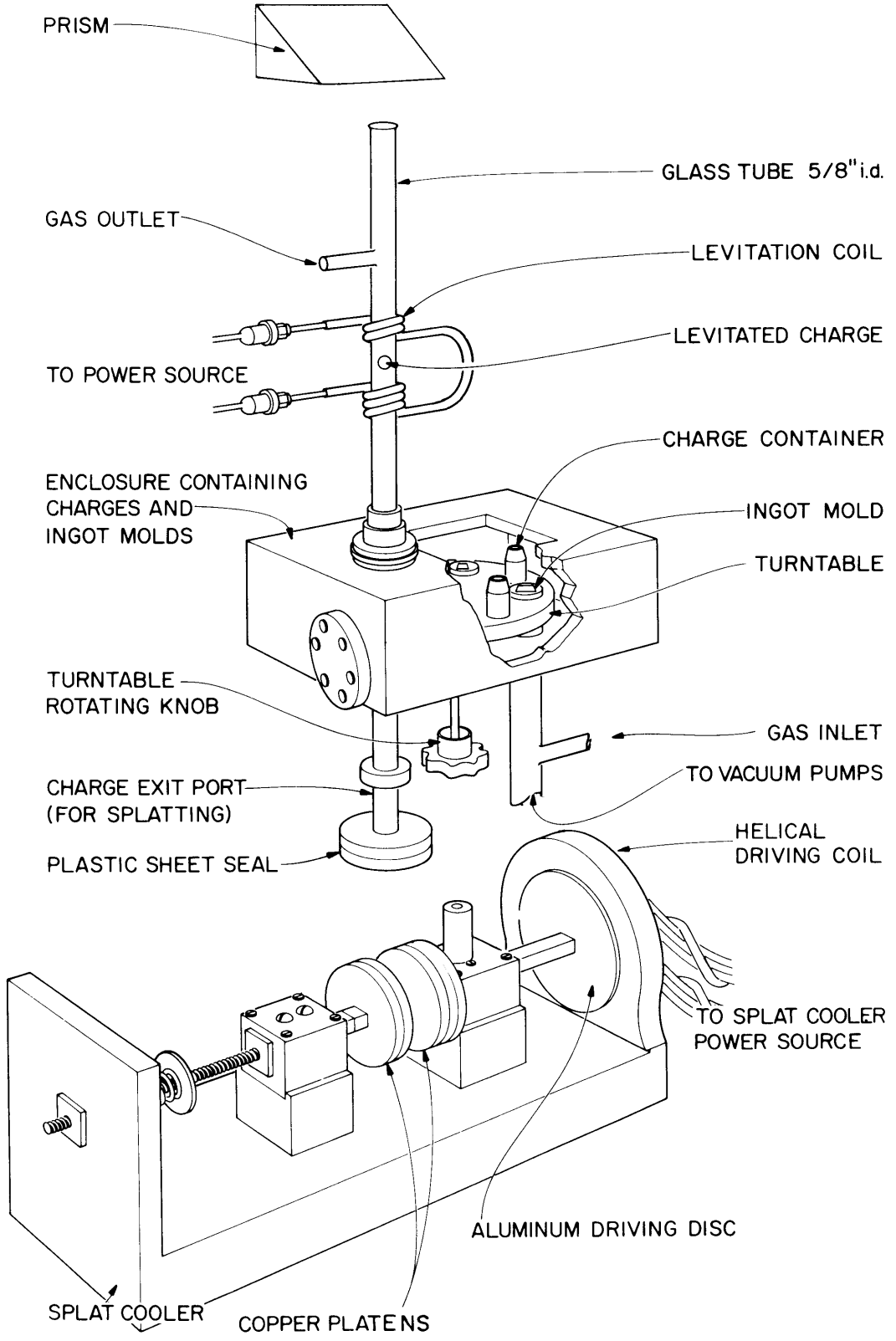

Figure 1. Sketch of levitation melting and casting apparatus.

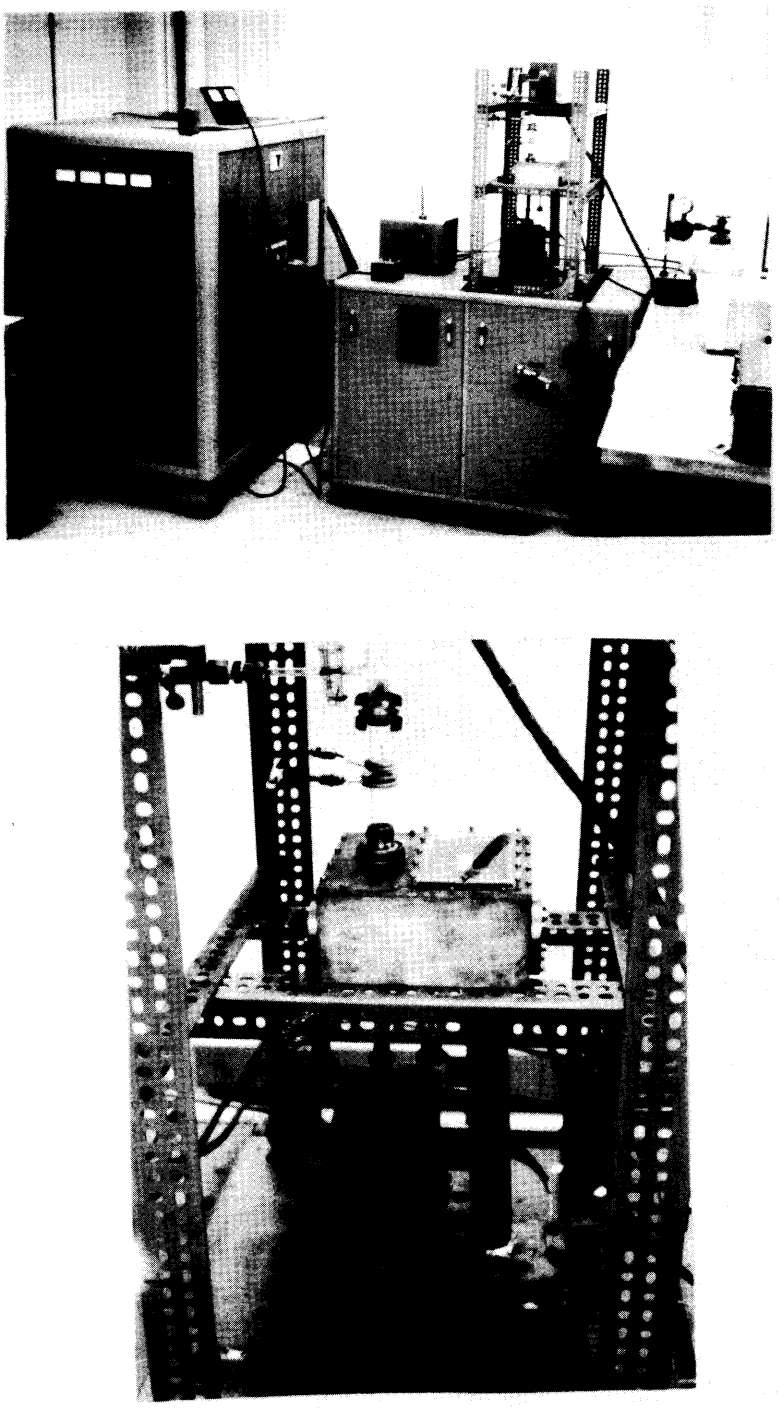

Figure 2. Photograph of levitation melting and casting apparatus.

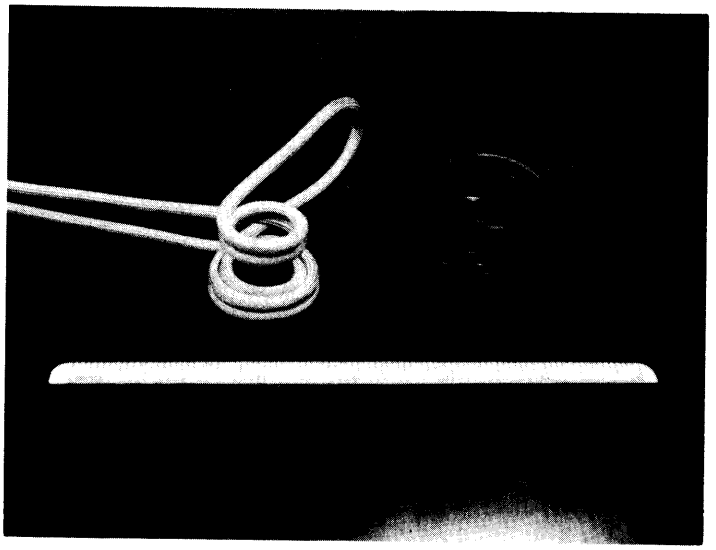

Figure 3. Photograph of levitation coils. Left: Coil for use with glass tube. Right: Conventional conical coil.

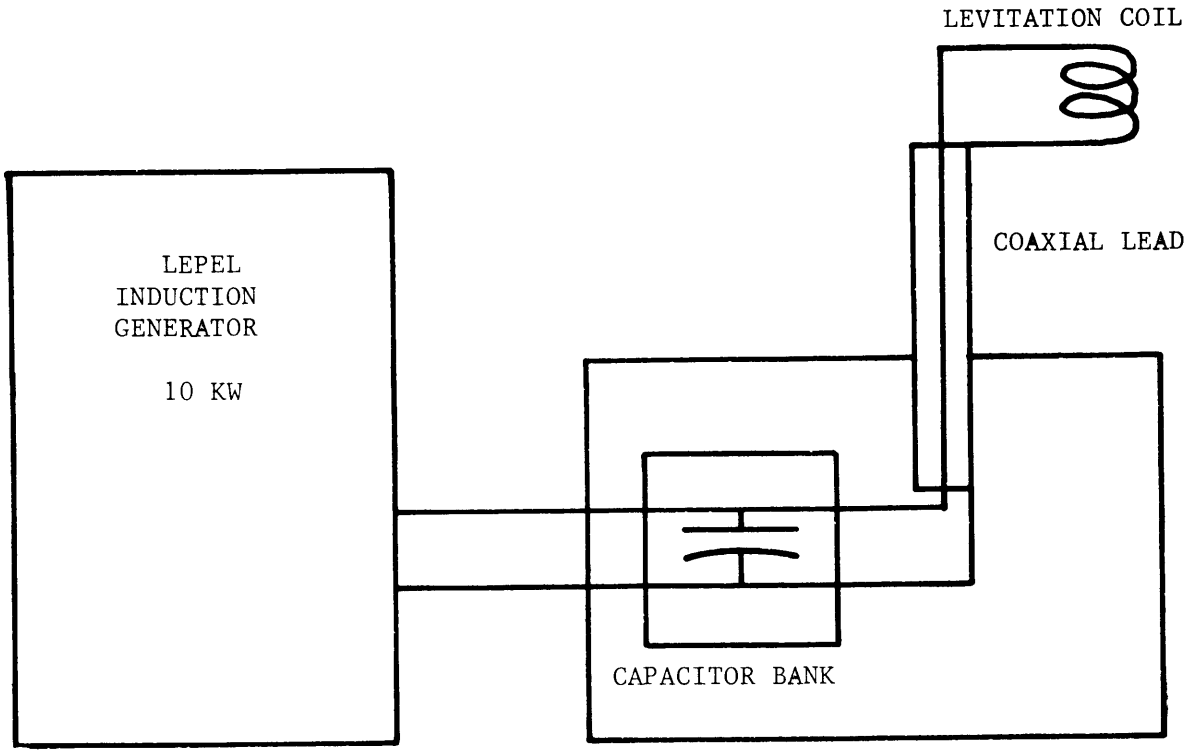

Figure 4. Schematic diagram of levitation melter circuit.

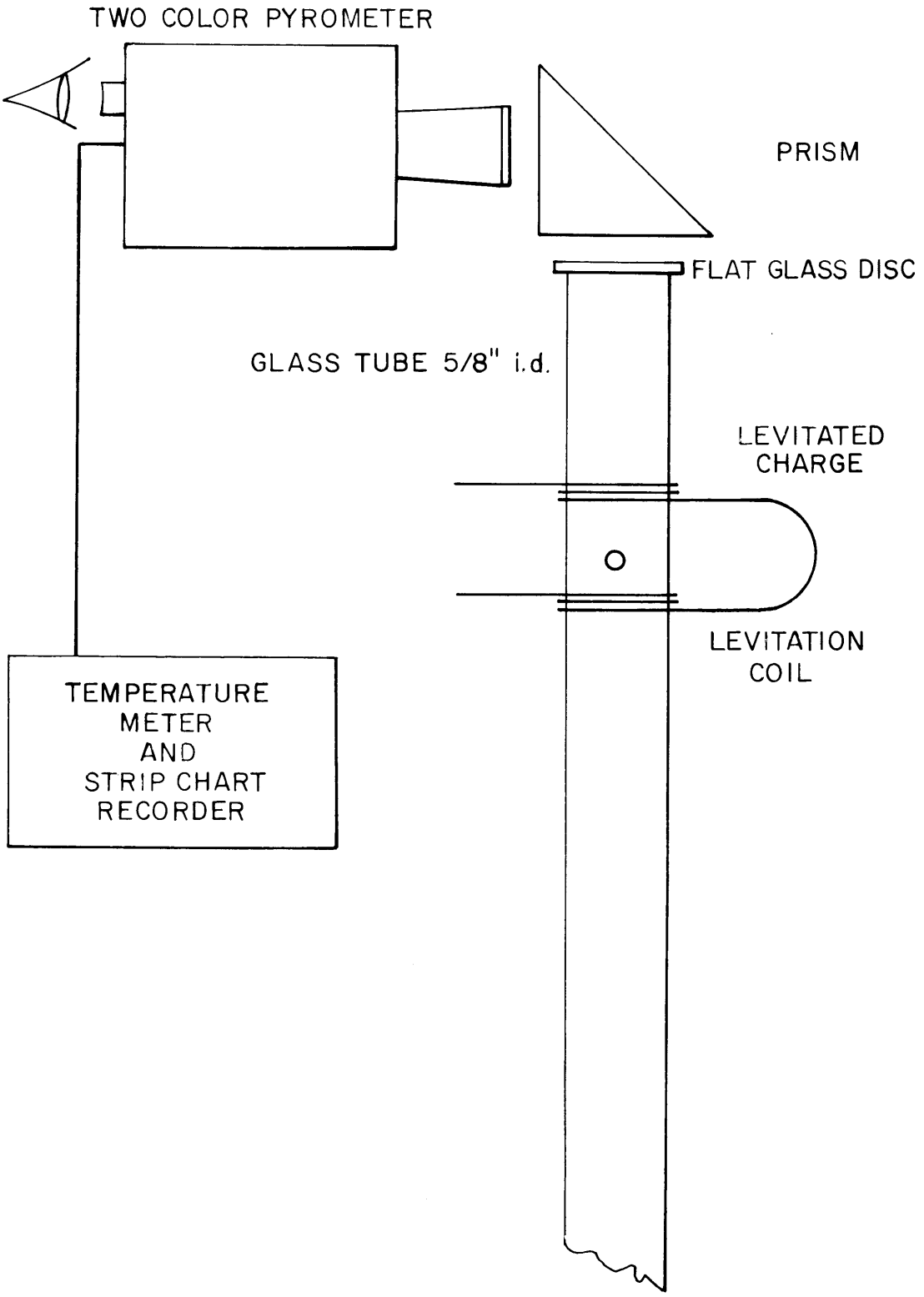

Figure 5. Schematic diagram of temperature measuring system.

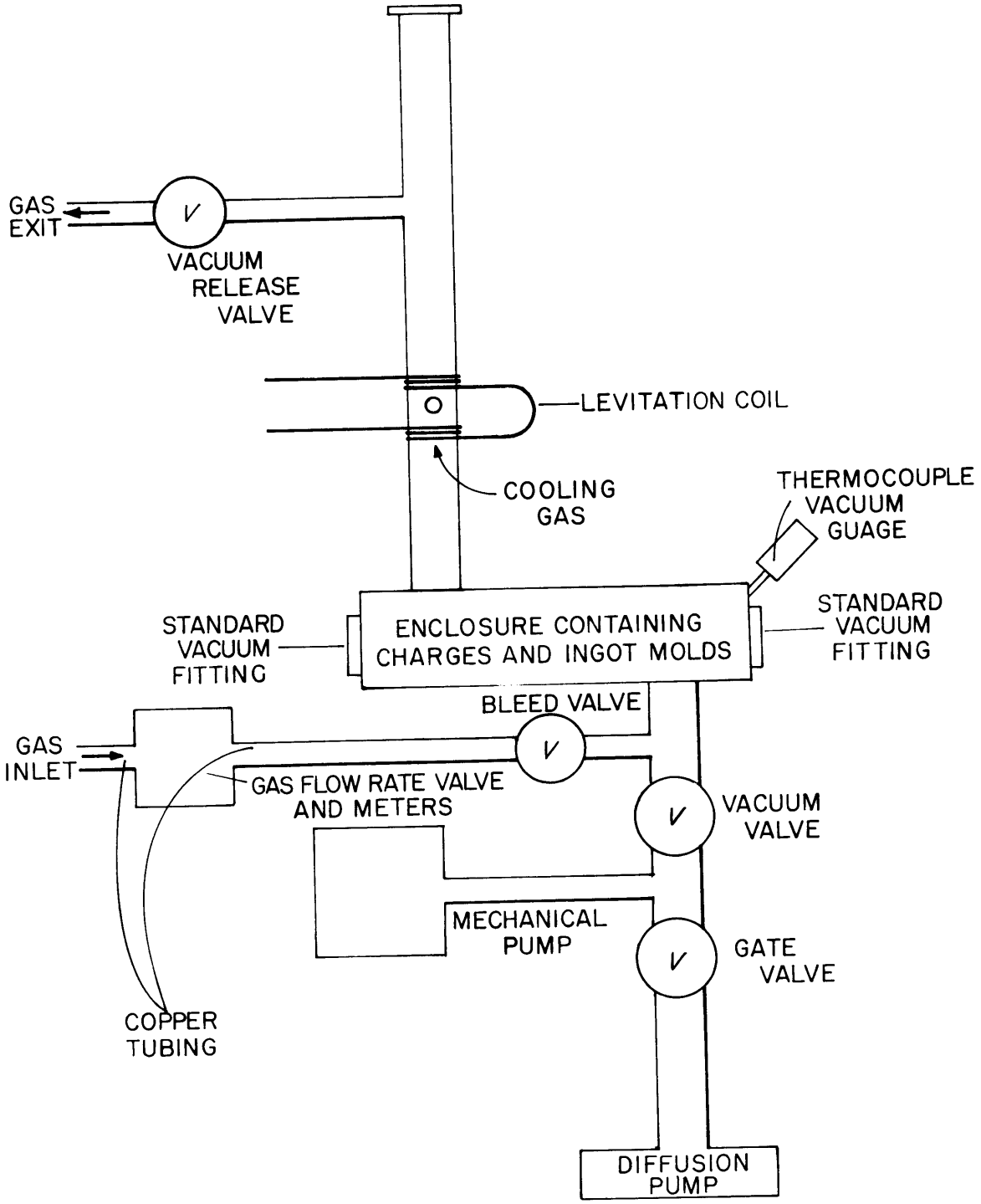

Figure 6. Schematic diagram of gas flow system.

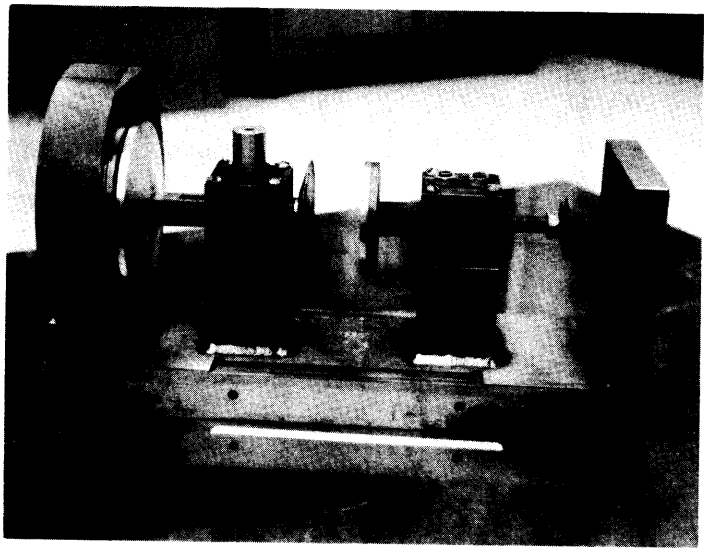

Figure 7. Photograph of "hammer and anvil".

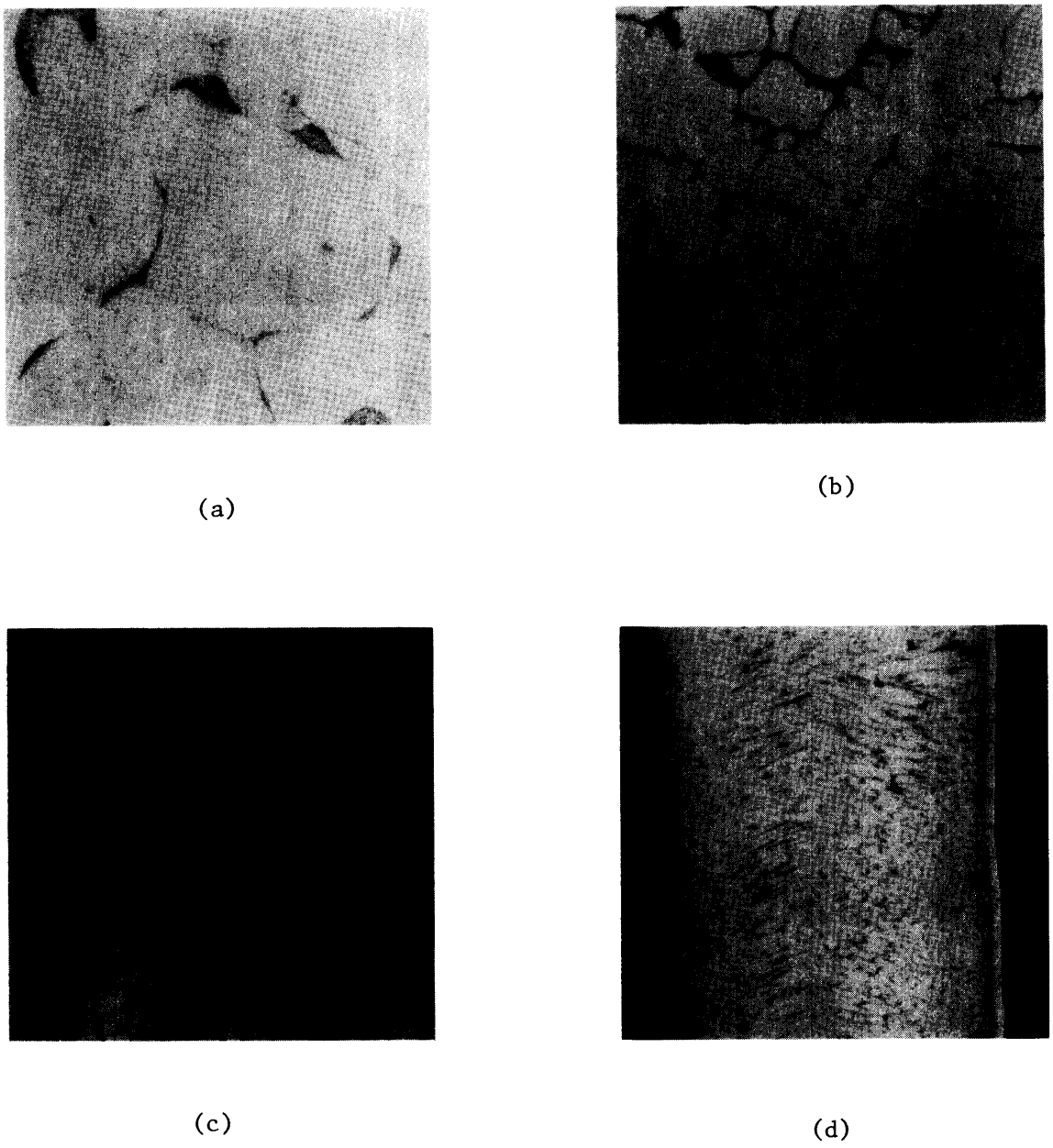

Figure 8. Variation of microstructure with cooling rate for 440C alloy. a) gas quench, b) liquid quench, c) chill cast, d) splat cooled. (500X, Murakami's etch).

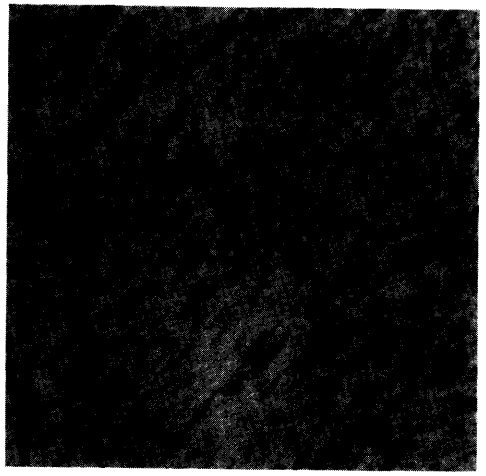

(a)

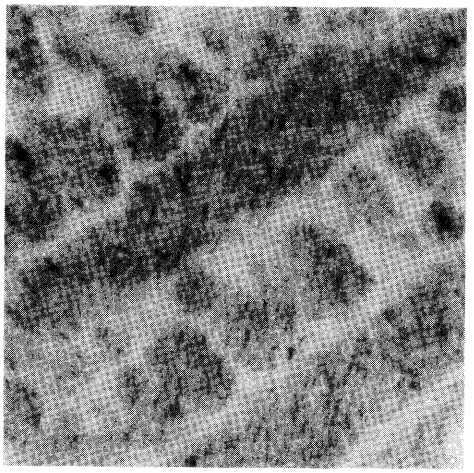

(b)

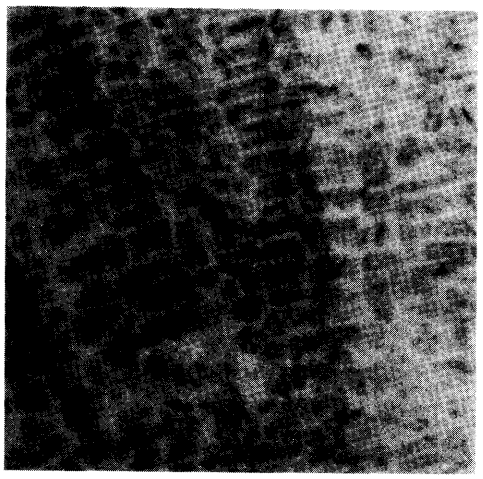

(c)

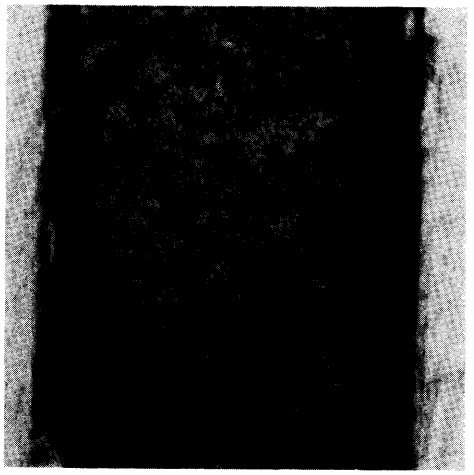

(d)

Figure 9. Variation of microstructure with cooling rate for 4330 alloy. a) gas quench, b) liquid quench, c) chill cast, d) splat cooled. (500X, Rosenhain's etch).

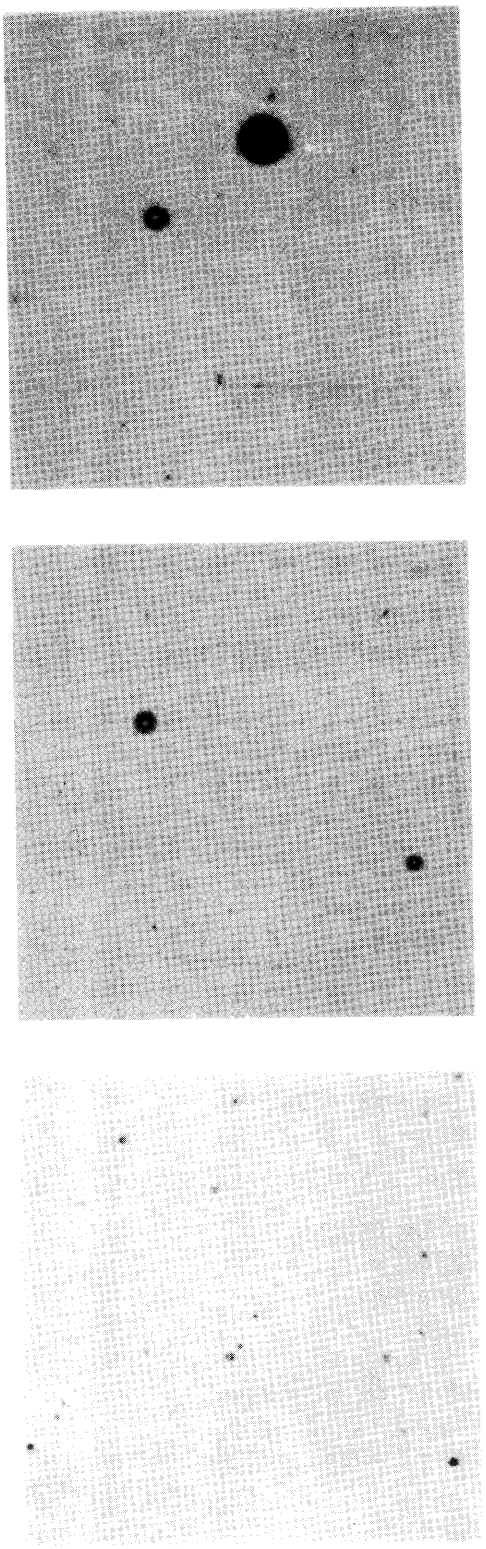

Figure 10. Variation of size and distribution of SiO_2 inclusions in an Fe-Si-O alloy.
TOP: Master alloy slowly solidified in vacuum induction furnace.
MIDDLE: Solidified in levitation coil with helium flow.
BOTTOM: Oil quenched.
(1000X).

Distribution List

	No. of Copies
Chief Office of Naval Research Department of the Navy Washington, D. C. 20360 Attn: Code 423	1
Commander U. S. Naval Research Laboratory Anacostia Station Washington, D. C. 20390 Attn: Technical Information Officer	1
Commanding General Deseret Test Center Fort Douglas, Utah 84113 Attn: Technical Information Office	1
Commanding General U. S. Army Electronics Command Fort Monmouth, New Jersey 07703 Attn: AMSEL-RD-MAT	2
Commanding General U. S. Army Materiel Command Washington, D. C. 20315 Attn: AMCRD-TC	1
Commanding General U. S. Army Missile Command Redstone Arsenal, Alabama 35809 Attn: Technical Library	1
Commanding General U. S. Army Munitions Command Dover, New Jersey 07801 Attn: Technical Library	1
Commanding General U.S. Army Tank-Automotive Command Warren, Michigan 48090 Attn: Tech. Data Coord. Br., SMOTA-RTS SMOTA-RCM.1	2 1
Commanding General U. S. Army Weapons Rock Island, Illinois 61201 Attn: Research & Development Directorate, AMSWE-RDR	1

Distribution List

	No. of Copies
Commanding General U. S. Army Satellite Communications Agency Fort Monmouth, New Jersey 07703 Attn: Technical Document Center	1
Commanding General White Sand Missile Range White Sands, New Mexico 88002 Attn: STEWS-WS-VT	1
Commanding Officer Aberdeen Proving Ground Maryland 21005 Attn: Technical Library, Bldg. 313	1
Commanding Officer U. S. Army Research Office (Durham) Box CM Duke Station Durham, North Carolina 27706	1
Commanding Officer Frankford Arsenal Bridge and Tacony Streets Philadelphia, Pennsylvania 19137 Attn: Library Branch, C-2500 Mr. H. Markus, SMUFA-L7000	1 1
Commanding Officer Picatinny Arsenal Dover, New Jersey 07801 Attn: SMUPA-VA6	1
Commanding Officer Watervliet Arsenal Watervliet, New York 12189 Attn: SWEWV-RDT, Technical Information Services Offices	1
Commanding Officer U. S. Army Aviation Materiel Laboratories Fort Eutstis, Virginia 23604	1
Commanding Officer USACDC Ordnance Agency Aberdeen Proving Ground, Maryland 21005 Attn: Library, Bldg. 305	2

Distribution List

	No. of Copies
Commanding Officer U. S. Army Edgewood Arsenal Edgewood Arsenal, Maryland 21010 Attn: Dir. of Eng. & Ind. Serv., Chem.-Mun Br., (Mr. F. E. Thompson)	1
Redstone Scientific Information Center U. S. Army Missile Command Redstone Arsenal, Alabama 35809 Attn: Chief, Documents Section	4
U. S. Army Aviation School Library USAAVNS-P&NRI Fort Rucker, Alabama 36360	1
Department of the Army Ohio River Division Laboratories Corps of Engineers 5851 Mariemont Avenue Cincinnati, Ohio 45227 Attn: ORDLB-TR	1
Commanding Officer Army Materials and Mechanics Research Center Watertown, Massachusetts 02172 Attn: AMXMR-AT, Technical Information Branch	5
AMXMR-AA	1
AMXMR-MX, Mr. N. Reed	1
AMXMR-RX, Dr. R. Beeuwkes, Jr.	1
AMXMR-RP, Mr. G. A. Darcy, Jr.	1
AMXMR-TP, Mr. P. A. G. Carbonaro	1
AMXMR-TP, Castings and Cermets Branch	5
Office of the Director Defense Research and Engineering The Pentagon Washington, D. C. 20301 Attn: Mr. J. C. Barrett	1
Dr. Donald MacArthur	1
Commander Defense Documentation Center Cameron Station, Bldg. 5 5010 Duke Station Alexandria, Virginia 22314	20

Distribution List

	No. of Copies
Defense Metals Information Center Battelle Memorial Institute Columbus, Ohio 43201	2
National Aeronautics and Space Administration Washington, D. C. 20546	
Attn: Mr. B. G. Achhammer	1
Mr. G. C. Deutsch	1
Mr. R. V. Rhode	1
National Aeronautics and Space Administration Marshall Space Flight Center Huntsville, Alabama 35812	
Attn: R-P&VE-M, Dr. W. Lucas	1
M-F&AE-M, Mr. W. A. Wilson, Bldg. 4720	1
Chief of Research and Development Department of the Army Washington, D. C. 20310	
Attn: Physical and Engineering Science Division	2
Air Force Materials Laboratory Wright-Patterson Air Force Base Ohio 45433	
Attn: AFML(MAA)	2
AFML(MAT)	1
AFML(MAM)	1
AFML(MAN)	1
American Foundrymen's Society Golf and Wolf Roads Des Plaines, Illinois 60016	
Attn: Mr. P. R. Gouwens	1
Case Institute of Technology University Circle Cleveland, Ohio 44106	
Attn: Professor J. F. Wallace	1
Dartmouth College Thayer School of Engineering Hanover, New Hampshire 03755	
Attn: Professor G. A. Colligan	1

Distribution List

	No. of Copies
Harvard University Cambridge, Massachusetts 02139 Attn: Professor Bruce Chalmers	1
Investment Casting Institute 3525 West Peterson Road Chicago, Illinois 60645 Attn: Mr. R. E. Pritchard	1
Massachusetts Institute of Technology Cambridge, Massachusetts 02139 Attn: Professor M. C. Flemings	
Northeastern University 360 Huntington Avenue Boston, Massachusetts 02115 Attn: Professor John Zotos	1
Steel Founders' Society Westview Towers 21010 Center Ridge Road Rocky River, Ohio 44116 Attn: Mr. Charles Briggs	1
Tufts University Medford, Massachusetts 02155 Attn: Professor K. Van Wormer, Jr.	1

DOCUMENT CONTROL DATA - R&D

(Security classification of title, body of abstract and indexing annotation must be entered when the overall report is classified)

1. ORIGINATING ACTIVITY (Corporate author)	2a. REPORT SECURITY CLASSIFICATION
Massachusetts Institute of Technology Cambridge, Massachusetts 02139	Unclassified
	2b. GROUP

3. REPORT TITLE

SOLIDIFICATION OF IRON BASE ALLOYS AT LARGE DEGREES OF UNDERCOOLING

4. DESCRIPTIVE NOTES (Type of report and inclusive dates)

Final Report, October 1, 1966 - December 31, 1967

5. AUTHOR(S) (Last name, first name, initial)

M. C. Flemings, M. Myers and W. E. Brower, Jr.

6. REPORT DATE	7a. TOTAL NO. OF PAGES	7b. NO. OF REFS
July 15, 1968	81	48

8a. CONTRACT OR GRANT NO.	9a. ORIGINATOR'S REPORT NUMBER(S)
DA-19-020-AMC-0231(X)	AMMRC CR 64-07/F
b. PROJECT NO. D/A 1C024401A328	
c. AMCMS Code 5025.11.294	9b. OTHER REPORT NO(S) (Any other numbers that may be assigned this report)
d.	

10. AVAILABILITY/LIMITATION NOTICES

This document has been approved for Public Release and Sale; its distribution is unlimited.

11. SUPPLEMENTARY NOTES	12. SPONSORING MILITARY ACTIVITY
	U.S. Army Materials & Mechanics Center, Watertown, Mass. 02172

13. ABSTRACT

Results are presented of isothermal holding experiments on Fe-50% Cu alloy with silica inclusions present. In addition to rapid dendrite coarsening, the inclusions are "pushed" by the growing dendrites; they collide, join and coalesce, and they coarsen by diffusion (Ostwald ripening). It is probable that similar effects occur during solidification of usual castings and ingots.

A levitation melting, undercooling, and splat cooling device has been modified to permit greater flexibility of operation and to incorporate ability to make chill plate castings (for study of mechanical properties as well as for structure). Dendrite arm spacing of commercial steel alloy castings made in this apparatus varies from about 50 microns for gas cooled specimens to less than 1 micron for splat cooled specimens. In work on Fe-Si-O alloy, no optically visible inclusions have been found in splat cooled samples.

DD FORM 1 JAN 64 1473

14. KEY WORDS	LINK A		LINK B		LINK C	
	ROLE	WT	ROLE	WT	ROLE	WT
Cast Steel Solidification Microsegregation Homogenization Inclusions						

INSTRUCTIONS

1. ORIGINATING ACTIVITY: Enter the name and address of the contractor, subcontractor, grantee, Department of Defense activity or other organization *(corporate author)* issuing the report.

2a. REPORT SECURITY CLASSIFICATION: Enter the overall security classification of the report. Indicate whether "Restricted Data" is included. Marking is to be in accordance with appropriate security regulations.

2b. GROUP: Automatic downgrading is specified in DoD Directive 5200.10 and Armed Forces Industrial Manual. Enter the group number. Also, when applicable, show that optional markings have been used for Group 3 and Group 4 as authorized.

3. REPORT TITLE: Enter the complete report title in all capital letters. Titles in all cases should be unclassified. If a meaningful title cannot be selected without classification, show title classification in all capitals in parenthesis immediately following the title.

4. DESCRIPTIVE NOTES: If appropriate, enter the type of report, e.g., interim, progress, summary, annual, or final. Give the inclusive dates when a specific reporting period is covered.

5. AUTHOR(S): Enter the name(s) of author(s) as shown on or in the report. Enter last name, first name, middle initial. If military, show rank and branch of service. The name of the principal author is an absolute minimum requirement.

6. REPORT DATE: Enter the date of the report as day, month, year; or month, year. If more than one date appears on the report, use date of publication.

7a. TOTAL NUMBER OF PAGES: The total page count should follow normal pagination procedures, i.e., enter the number of pages containing information.

7b. NUMBER OF REFERENCES: Enter the total number of references cited in the report.

8a. CONTRACT OR GRANT NUMBER: If appropriate, enter the applicable number of the contract or grant under which the report was written.

8b, 8c, & 8d. PROJECT NUMBER. Enter the appropriate military department identification, such as project number, subproject number, system numbers, task number, etc.

9a. ORIGINATOR'S REPORT NUMBER(S): Enter the official report number by which the document will be identified and controlled by the originating activity. This number must be unique to this report.

9b. OTHER REPORT NUMBER(S): If the report has been assigned any other report numbers *(either by the originator or by the sponsor)*, also enter this number(s).

10. AVAILABILITY/LIMITATION NOTICES: Enter any limitations on further dissemination of the report, other than those imposed by security classification, using standard statements such as:

(1) "Qualified requesters may obtain copies of this report from DDC."

(2) "Foreign announcement and dissemination of this report by DDC is not authorized."

(3) "U. S. Government agencies may obtain copies of this report directly from DDC. Other qualified DDC users shall request through _____."

(4) "U. S. military agencies may obtain copies of this report directly from DDC. Other qualified users shall request through _____."

(5) "All distribution of this report is controlled. Qualified DDC users shall request through _____."

If the report has been furnished to the Office of Technical Services, Department of Commerce, for sale to the public, indicate this fact and enter the price, if known.

11. SUPPLEMENTARY NOTES: Use for additional explanatory notes.

12. SPONSORING MILITARY ACTIVITY: Enter the name of the departmental project office or laboratory sponsoring *(paying for)* the research and development. Include address.

13. ABSTRACT: Enter an abstract giving a brief and factual summary of the document indicative of the report, even though it may also appear elsewhere in the body of the technical report. If additional space is required, a continuation sheet shall be attached.

It is highly desirable that the abstract of classified reports be unclassified. Each paragraph of the abstract shall end with an indication of the military security classification of the information in the paragraph, represented as *(TS)*, *(S)*, *(C)*, *or (U)*.

There is no limitation on the length of the abstract. However, the suggested length is from 150 to 225 words.

14. KEY WORDS: Key words are technically meaningful terms or short phrases that characterize a report and may be used as index entries for cataloging the report. Key words must be selected so that no security classification is required. Identifiers, such as equipment model designation, trade name, military project code name, geographic location, may be used as key words but will be followed by an indication of technical context. The assignment of links, rules, and weights is optional.

AD_____ Accession No. _____

U.S. Materials and Mechanics Center, Watertown, Massachusetts 02172

SOLIDIFICATION OF IRON BASE ALLOYS AT LARGE DEGREES OF UNDERCOOLING

M. C. Flemings, M. Myers, and W. E. Brower, Jr.

Report AMMRC CR 64-07/F, Oct 1966 - Dec 1967, 81 pp - tables - illus, AMCMS Code No. 5025.11.294, D/A Project No. 1C024401A328, Unclassified report.

Results are presented of isothermal holding experiments on Fe-50% Cu alloy with silica inclusions present. In addition to rapid dendrite coarsening, the inclusions are "pushed" by the growing dendrites; they collide, join and coalesce, and they coarsen by diffusion (Ostwald ripening). It is probable that similar effects occur during solidification of usual castings and ingots.

A levitation melting, undercooling, and splat cooling device has been modified to permit greater felxibility of operation and to incorporate ability to make chill plate castings (for study of mechanical properties as well as for structure). Dendrite arm spacing of commercial steel alloy castings made in this apparatus varies from about 50 microns for gas cooled specimens to less than 1 micron for splat cooled specimens. In work on Fe-Si-O alloy, no optically visible inclusions have been found in splat cooled samples.

NO DISTRIBUTION LIMITATIONS

UNCLASSIFIED

1. Cast Steel
2. Microsegregation
3. Solidification
4. Homogenization

I. M. C. Flemings
M. Myers
W. E. Brower, Jr.

II. AMCMS Code No. 5025.11.294

III. D/A Project No. 1C024401A328

AD_____ Accession No. _____

U.S. Materials and Mechanics Center, Watertown, Massachusetts 02172

SOLIDIFICATION OF IRON BASE ALLOYS AT LARGE DEGREES OF UNDERCOOLING

M. C. Flemings, M. Myers, and W. E. Brower, Jr.

Report AMMRC CR 64-07/F, Oct 1966 - Dec 1967, 81 pp - tables - illus, AMCMS Code No. 5025.11.294, D/A Project No. 1C024401A328, Unclassified report.

Results are presented of isothermal holding experiments on Fe-50% Cu alloy with silica inclusions present. In addition to rapid dendrite coarsening, the inclusions are "pushed" by the growing dendrites; they collide, join and coalesce, and they coarsen by diffusion (Ostwald ripening). It is probable that similar effects occur during solidification of usual castings and ingots.

A levitation melting, undercooling, and splat cooling device has been modified to permit greater felxibility of operation and to incorporate ability to make chill plate castings (for study of mechanical properties as well as for structure). Dendrite arm spacing of commercial steel alloy castings made in this apparatus varies from about 50 microns for gas cooled specimens to less than 1 micron for splat cooled specimens. In work on Fe-Si-O alloy, no optically visible inclusions have been found in splat cooled samples.

NO DISTRIBUTION LIMITATIONS

UNCLASSIFIED

1. Cast Steel
2. Microsegregation
3. Solidification
4. Homogenization

I. M. C. Flemings
M. Myers
W. E. Brower, Jr.

II. AMCMS Code No. 5025.11.294

III. D/A Project No. 1C024401A328

AD_____ Accession No. _____

U.S. Materials and Mechanics Center, Watertown, Massachusetts 02172

SOLIDIFICATION OF IRON BASE ALLOYS AT LARGE DEGREES OF UNDERCOOLING

M. C. Flemings, M. Myers, and W. E. Brower, Jr.

Report AMMRC CR 64-07/F, Oct 1966 - Dec 1967, 81 pp - tables - illus, AMCMS Code No. 5025.11.294, D/A Project No. 1C024401A328, Unclassified report.

Results are presented of isothermal holding experiments on Fe-50% Cu alloy with silica inclusions present. In addition to rapid dendrite coarsening, the inclusions are "pushed" by the growing dendrites; they collide, join and coalesce, and they coarsen by diffusion (Ostwald ripening). It is probable that similar effects occur during solidification of usual castings and ingots.

A levitation melting, undercooling, and splat cooling device has been modified to permit greater felxibility of operation and to incorporate ability to make chill plate castings (for study of mechanical properties as well as for structure). Dendrite arm spacing of commercial steel alloy castings made in this apparatus varies from about 50 microns for gas cooled specimens to less than 1 micron for splat cooled specimens. In work on Fe-Si-O alloy, no optically visible inclusions have been found in splat cooled samples.

NO DISTRIBUTION LIMITATIONS

UNCLASSIFIED

1. Cast Steel
2. Microsegregation
3. Solidification
4. Homogenization

I. M. C. Flemings
M. Myers
W. E. Brower, Jr.

II. AMCMS Code No. 5025.11.294

III. D/A Project No. 1C024401A328

AD_____ Accession No. _____

U.S. Materials and Mechanics Center, Watertown, Massachusetts 02172

SOLIDIFICATION OF IRON BASE ALLOYS AT LARGE DEGREES OF UNDERCOOLING

M. C. Flemings, M. Myers, and W. E. Brower, Jr.

Report AMMRC CR 64-07/F, Oct 1966 - Dec 1967, 81 pp - tables - illus, AMCMS Code No. 5025.11.294, D/A Project No. 1C024401A328, Unclassified report.

Results are presented of isothermal holding experiments on Fe-50% Cu alloy with silica inclusions present. In addition to rapid dendrite coarsening, the inclusions are "pushed" by the growing dendrites; they collide, join and coalesce, and they coarsen by diffusion (Ostwald ripening). It is probable that similar effects occur during solidification of usual castings and ingots.

A levitation melting, undercooling, and splat cooling device has been modified to permit greater felxibility of operation and to incorporate ability to make chill plate castings (for study of mechanical properties as well as for structure). Dendrite arm spacing of commercial steel alloy castings made in this apparatus varies from about 50 microns for gas cooled specimens to less than 1 micron for splat cooled specimens. In work on Fe-Si-O alloy, no optically visible inclusions have been found in splat cooled samples.

NO DISTRIBUTION LIMITATIONS

UNCLASSIFIED

1. Cast Steel
2. Microsegregation
3. Solidification
4. Homogenization

I. M. C. Flemings
M. Myers
W. E. Brower, Jr.

II. AMCMS Code No. 5025.11.294

III. D/A Project No. 1C024401A328

AD_____ Accession No. _____
U.S. Materials and Mechanics Center, Watertown, Massachusetts 02172
SOLIDIFICATION OF IRON BASE ALLOYS AT LARGE DEGREES OF UNDERCOOLING
M. C. Flemings, M. Myers, and W. E. Brower, Jr.

Report AMMRC CR 64-07/F, Oct 1966 - Dec 1967, 81 pp - tables - illus, AMCMS Code No. 5025.11.294, D/A Project No. 1C024401A328, Unclassified report.

Results are presented of isothermal holding experiments on Fe-50% Cu alloy with silica inclusions present. In addition to rapid dendrite coarsening, the inclusions are "pushed" by the growing dendrites; they collide, join and coalesce, and they coarsen by diffusion (Ostwald ripening). It is probable that similar effects occur during solidification of usual castings and ingots.

A levitation melting, undercooling, and splat cooling device has been modified to permit greater felxibility of operation and to incorporate ability to make chill plate castings (for study of mechanical properties as well as for structure). Dendrite arm spacing of commercial steel alloy castings made in this apparatus varies from about 50 microns for gas cooled specimens to less than 1 micron for splat cooled specimens. In work on Fe-Si-O alloy, no optically visible inclusions have been found in splat cooled samples.

NO DISTRIBUTION LIMITATIONS

UNCLASSIFIED

1. Cast Steel
2. Microsegregation
3. Solidification
4. Homogenization

I. M. C. Flemings
M. Myers
W. E. Brower, Jr.

II. AMCMS Code No. 5025.11.294

III. D/A Project No. 1C024401A328

AD_____ Accession No. _____
U.S. Materials and Mechanics Center, Watertown, Massachusetts 02172
SOLIDIFICATION OF IRON BASE ALLOYS AT LARGE DEGREES OF UNDERCOOLING
M. C. Flemings, M. Myers, and W. E. Brower, Jr.

Report AMMRC CR 64-07/F, Oct 1966 - Dec 1967, 81 pp - tables - illus, AMCMS Code No. 5025.11.294, D/A Project No. 1C024401A328, Unclassified report.

Results are presented of isothermal holding experiments on Fe-50% Cu alloy with silica inclusions present. In addition to rapid dendrite coarsening, the inclusions are "pushed" by the growing dendrites; they collide, join and coalesce, and they coarsen by diffusion (Ostwald ripening). It is probable that similar effects occur during solidification of usual castings and ingots.

A levitation melting, undercooling, and splat cooling device has been modified to permit greater felxibility of operation and to incorporate ability to make chill plate castings (for study of mechanical properties as well as for structure). Dendrite arm spacing of commercial steel alloy castings made in this apparatus varies from about 50 microns for gas cooled specimens to less than 1 micron for splat cooled specimens. In work on Fe-Si-O alloy, no optically visible inclusions have been found in splat cooled samples.

NO DISTRIBUTION LIMITATIONS

UNCLASSIFIED

1. Cast Steel
2. Microsegregation
3. Solidification
4. Homogenization

I. M. C. Flemings
M. Myers
W. E. Brower, Jr.

II. AMCMS Code No. 5025.11.294

III. D/A Project No. 1C024401A328